Title: Routes of phlogopite weathering by three fungal strains

Short Running title: Phlogopite fungal weathering

Authors:

Flavia Pinzari[1,3], Javier Cuadros[2], Rosario Napoli[1], Loredana Canfora[1], David Baussà Bardají[2]

Affiliations:

[1]Consiglio per la ricerca in agricoltura e l'analisi dell'economia agraria. Centro Agricoltura Ambiente. Via della Navicella 2-4, 00184 Rome, Italy

[2]Department of Earth Sciences, Natural History Museum, Cromwell Road, SW7 5BD London, UK

[3]Department of Life Sciences, Natural History Museum, Cromwell Road, SW7 5BD London, UK

Corresponding author:

Flavia Pinzari
Consiglio per la ricerca in agricoltura e l'analisi dell'economia agraria
Centro Agricoltura Ambiente
Via della Navicella, 2-4
00184 Rome, Italy
flavia.pinzari@crea.gov.it

Scientific Associate
Department of Life Sciences
Natural History Museum of London
f.pinzari@nhm.ac.uk

mobile +39 3475255938

Abstract

Fungi dissolve soil minerals by acidifying their microenvironments, exuding chelating molecules, and by mechanical disruption of the crystal lattice. Dissolution may occur at two scales: microscale (surface of contact between fungus and mineral) and medium scale (affecting entire mineral grains). Mineral weathering by fungi and other microorganisms is being intensely investigated as thought to be a significant global contribution to weathering, perhaps also modifying weathering products, especially clay minerals. Here we report fungal dissolution of phlogopite (Mg-Fe-rich mica) in experiments with three fungal strains (*Alternaria tenuissima*, *Cladosporium cladosporioides* and *Stilbella* sp.) grown on solid medium for 30 days at 21 °C and 96-100% relative humidity. The focus was to investigate the chemical changes induced by the fungi on phlogopite, translocation of micronutrients to the mycelium and the possible differences between the three species. The study used variable-pressure SEM-EDS equipped with both secondary electrons with charge contrast imaging and backscattered electrons. Statistical analysis of the results (principal component and discriminant analysis) discriminated between the weathering activities of the three fungal species, which increased from *Stilbella* to *C. cladosporioides* to *A. tenuissima*, in agreement with the respective decreasing pH values measured in the media (6.4, 5.8, 5.2 ± 0.03). Phlogopite weathering features were irregular and variable (contrast change, troughs, lateral dissolution, flake thinning, breakdown), apparently not caused by direct contact with fungal hyphae. EDS values indicated several weathering stages and two or more dissolution mechanisms, one of them suggesting cation rearrangement in the mica towards decreasing octahedral and interlayer cation contents that produced Al-rich smectite. Intimate fungus-mineral interaction was observed as hyphal attachment to phlogopite surfaces, penetration between sheets at the edges (where phlogopite structure is more labile) and changes in the

contrast of the mica surface around attached hyphae. The lack of observable dissolution traces from such contact interaction is interpreted as the result of effacing by the more intense acid leaching operating at larger scale.

Key words: Bioweathering, fungi, geomicrobiology, phlogopite, SEM-EDS.

1. Introduction

Jongmans *et al.* (1997) coined the term "rock-eating fungi" in connection with the microscopic tunnels documented within feldspar and hornblende grains in the E horizon of podzol soils (Driessen *et al.*, 2001). These microscopic tunnels were the effect of mineral dissolution by fungi in order to obtain nutrients. Several authors showed that fungi, especially ectomycorrhizal species, are able to actively weather silicate minerals to extract nutrients like P, K, Ca, Mg and Fe, in particular under conditions of nutrient limitation (Boyle & Voigt, 1973; Leyval & Berthelin, 1991; Paris *et al.*, 1995, 1996; Jongmans *et al*., 1997; Wallander & Wickman, 1999; Crawford *et al.*, 2000; Blum *et al.*, 2002; Burford *et al.*, 2003a; Yuan *et al.*, 2004; Rosling *et al.*, 2004a; Balogh-Brunstad *et al.*, 2008a, 2008b; Arocena *et al.* 2012). Arocena *et al.* (2012) proposed that mycorrhizal fungi selectively extract K from biotite flakes. In agreement with this, the uptake of K by plants was reported to convert phlogopite (Mg and Fe-rich mica) into vermiculite, an expandable phyllosilicate of high interlayer charge (Hinsinger *et al.*, 2006). Vermiculite was also produced by selective and biologically-mediated removal of Mg from chlorite, a Mg-rich phyllosilicate mineral typically generated at high temperature (Arocena & Velde, 2009). *In vitro* studies showed dissolution channels on biotite flakes accompanied by depletion of K and the oxidation of iron from Fe (II) to Fe (III) (Balogh-Brunstad *et al.*, 2008a, 2008b). However, the dissolving action of fungi to extract mineral nutrients does not exclusively take place at the microscale, generating tunnels or

similar structures. A survey by Hoffland *et al*. (2004, 2005) on 75 soils from Europe, Asia, North America and Australia indicated that tunnelled minerals occur almost exclusively in podzols in temperate and boreal zones, and sometimes in acid brown forest soils. There are then other forms of fungal dissolution of minerals which operate at medium scale and result in general mineral grain dissolution.

Experimental studies have shown that both free-living fungi and plant symbionts use the micro and the medium scale attack types. Some of the several described mechanisms of mineral dissolution by fungi could operate at both medium and microscale, and result in general dissolution features or in channel or tunnel formation. This is the case of acidification of the microenvironment via excretion of protons, phosphoric acid, organic acids, CO_2 (Burgstaller & Schinner, 1993; Arvieu *et al.*, 2003; Fomina *et al.*, 2006; Wallander, 2006; Balogh-Brunstad *et al.*, 2008a); production of extracellular polymeric substances that adsorb and accumulate cations and decrease the saturation for those elements (Welch & Vandevivere, 1994; Barker & Banfield, 1996; Barker *et al.*, 1997; Banfield *et al.*, 1999; Gadd, 1999; Bray *et al*., 2015); exudation of organic complex-forming molecules (Adeyemi & Gadd, 2005; Bray *et al*., 2015); modification of water chemistry (e.g., concentrating salts) and/or viscosity within biofilms that increases water reactivity with the mineral surface (Cuadros *et al*., 2013). Other mechanisms, however, appear to be linked to the direct fungal action on the mineral surface. Several studies emphasized the potential importance of localized microbial effects on mineral dissolution caused by surface attachment (Jongmans *et al*., 1997; Barker *et al*., 1997; Banfield *et al*., 1999; Rosling *et al*., 2004b), and the exchange of protons for base cations at the attachment locus (Jenny, 1980; Fomina *et al*., 2006; Wallander, 2006; Balogh-Brunstad *et al*., 2008b). According to Gazzè *et al*. (2012) the weathering of minerals by fungi may also have a mechanical nature since the internal pressure in hyphae can reach values between 0.4

and 8 MPa, and can produce structural alterations of phyllosilicates (Bonneville *et al*., 2009), possibly by causing strain in the mineral during hyphal growth. The above mechanisms of fungal dissolution of minerals have been summarized by Fomina *et al.* (2007), who categorize them as biomechanical and biochemical, the latter produced by acidolysis and complexolysis. In any event the biomechanical weathering also depends strongly on biochemical processes.

Fungal capacity to dissolve minerals has been mainly investigated in order to establish the overall ability of fungi to extract nutrients from the minerals (Barker *et al*., 1997; Hopf *et al*., 2009; Paris *et al*., 1995; Yuan *et al*., 2004). The more restricted attention to dissolution mechanisms has resulted in a limited documentation of microscale tracks on mineral surfaces (Bonneville *et al*., 2009; Gazzè *et al*., 2012). Balogh-Brunstad *et al*. (2008b) observed that fungal action in liquid culture caused K, Mg and Fe removal from biotite and incorporation into fungal biomass without production of SEM-detectable marks on the mineral surface. Saccone *et al*. (2009) also described a dissolution mechanism for hornblende colonized *in vitro* by symbiotic *P. involutus* that did not result in surface marks but in the generalized weakening of the mineral structure. On the contrary, Gazzè *et al.* (2012) found channels ~1 μm wide and up to 50 nm deep on the surface of chlorite after contact with symbiotic ectomycorrhizal fungi using atomic force microscopy. The morphology of the channels indicated a fungal-induced origin. In experiments with lizardite, Li *et al*. (2016) found that only attached fungal cells released siderophores that, in conjunction with biomechanical forces and local acidification, produced Fe loss exclusively at the cell-mineral interface.

At the present stage it is difficult to assess whether fungal attack on minerals is more frequent through channelling/tunnelling or through global grain dissolution because there are no sufficient studies for this evaluation. Balogh-Brunstad *et al*. (2008b) indicated that only 1% of the dissolution in their experiments with liquid-medium cultures took place by the generation

of channels on the surface of biotite, with 99% due to global dissolution. Water saturated conditions in their experiments could be the reason for low dissolution by contact with fungal hyphae, because water and nutrient limitation probably foster direct hyphal dissolution (Hoffland *et al*., 2004; Balogh-Brunstad *et al*., 2008b). However, also in water saturation conditions, Li *et al*. (2016) found a much larger fraction of dissolution, 40-50%, produced by direct contact between mineral and fungus. Apparently, the relative extent of microscale and medium scale weathering processes depends on multiple factors that include the above mentioned water and nutrient availability and perhaps others such as mineral particle size and shape, water mobility and fungal distribution in the soil.

Scanning electron microscopy (SEM) has been used extensively for the visualisation of fungi in association with minerals (Fomina *et al*., 2005; Gleeson *et al*., 2005; Burford *et al*., 2006; Rosling *et al*., 2007) because it can provide spatial information at the micrometer to sub-micrometer scales and, coupled with energy-dispersive X-ray spectroscopy (EDS), it can reveal high-resolution elemental compositional measurements. Here we report phlogopite dissolution mediated by three fungal strains in experiments performed using surface growth on solid (agar) medium. The aims of this study were first to investigate changes in the morphology and elemental composition of mica flakes using SEM-EDS and second to document the mobilization of microelements from the minerals to the mycelium.

2. Materials and methods

2.1 *Mica*

Phlogopite samples were collected in a volcanic area in Manziana (near Rome, Italy; 42°05'11.8"N 12°06'05.5"E) close to "Caldara di Manziana", a protected natural area (coded as a SIC, IT6030009, in 2006/613/CE). Caldara di Manziana is a subcircular structure of 0.25

161 km^2 generated during the alkalipotassic volcanism affecting central Italy since 0.6 Ma. The
162 origin of this structure may have been a hydrothermal explosion but is still debated (Costa el
163 al., 2008). The phlogopite consists of cm-sized sheets of 1-2 mm thickness virtually free from
164 other minerals (Figure 1a, 1b). These sheets were cleaned with distilled water and cut or
165 separated into 1-2 cm pieces. These were water steam sterilized (10 min at 121°C). The
166 temperature and time used in the sterilization are too low and short, respectively, to cause any
167 change in phlogopite (Mackenzie, 1970). The use of chemicals would not have ensured the
168 complete elimination of resistant bacteria (Thomas, 2012). Comparison of the phlogopite
169 surface and chemistry before and after the sterilization process showed not changes.
170
171 2.2 *Fungal strains and identification*
172 Three fungal strains that had originally been isolated from soils and incorporated into the
173 CREA-RPS (Rome, Italy) culture collection were used to inoculate the samples. The identity
174 of the strains was already known and it was confirmed immediately before the experiments
175 with molecular biological methods. The fungi were *Cladosporium*, *Alternaria* and *Stilbella*
176 isolates, all of which are common in soils (Foster & Bills, 2011). They were selected because
177 it was expected, according to available literature and preliminary tests, that they would
178 promote different ways of mineral alteration.
179
180 The identification of the fungal strains was confirmed by sequencing the ITS1-ITS4 regions
181 of the rDNA (White *et al.*, 1990). The β-tubulin gene sequence was also used in the case of
182 the *Stilbella* strain, since it did not produce diagnostic conidiophora and conidia, and its ITS1-
183 ITS4 region was not decisive for identification. The β-tubulin gene was amplified using the
184 primer pair Bt2 (Bt2a-Bt2b) developed by Glass and Donaldson (1995). PCR reactions were
185 performed in a Biorad Mini Opticon unit using Phusion hot start Taq DNA Polymerase

(Platinum, Invitrogen). Purified sequences were despatched for sequencing (MWG, Germany). The forward and reverse electropherograms obtained for each fungal isolate were verified visually and aligned using CLUSTALW (version 2.0) to obtain consensus sequences that were then compared using the BLAST search program (Altschul *et al.*, 1997) with the NCBI (Karsch-Mizrachi *et al.*, 2012) and UNITE databases (Koljalg *et al.*, 2005; Abarenkov *et al.*, 2010).

Both *Alternaria* and *Cladosporium* species have been recorded as rock-eating fungi (Burford *et al.*, 2003b). *Alternaria* species can alter rocks with direct enzymatic mechanisms (Gadd & Sayer, 2000), produce organic acids (Lou *et al.*, 2013) and, according to Gadd & Sayer (2000), can mediate methylation of metals under aerobic conditions. *Cladosporium* species secrete organic acids (Sterflinger, 2000) and were found associated to sandstone, marble, granite and andesite (Burford *et al.*, 2003a). *Stilbella* species were found to possess enzymes catalyzing the dismutation (or partitioning) of the superoxide (O_2^-) radical into either ordinary molecular oxygen (O_2) or hydrogen peroxide (H_2O_2). Extracellular superoxide (O_2^-) was identified as the oxidant of Mn(II) to Mn(III) in the species *Stilbella aciculosa* (Hansel *et al.*, 2012).

2.3 Culturing methods

The phlogopite flakes were placed on a disk of Whatman 1CHR paper (ash free, Cat. N8 3001 917; chromatography grade) inside a 5 cm diameter polystyrene Petri dish containing 2% ash free microbiological agar (Oxoid, Thermo Scientific bacteriological Agar n.1, Code: LP0011, a processed agar with low Ca and Mg levels) to keep the microcosm moist but not soaked with water. The agar contained 0.4 g/l of potato extract and 2 g/l of glucose (corresponding to a 10 fold diluted formulation of Potato Dextrose Agar, PDA) (Oxoid, Thermo Scientific, code

CM0139) to provide vitamins and organic nutrients for initial fungal growth, in case cellulose was not readily degradable by the fungal strain. The elemental composition of the PDA medium, as measured with SEM-EDS in the powders, is provided in the Supplementary data, Table S1.

Inoculums were obtained from 7-day old PDA cultures. The fungal mycelium was inoculated in three or four points at 0.5 cm from the mica flakes already positioned on the agar in the Petri dish. Three replicates were prepared for each fungus-mica experiment. The Petri dishes were incubated for 30 days at 21±1 °C and ~100% relative humidity in a controlled environment (RH monitored with a Hygrolog-D Rotronic sensor, Bassersdorf, Switzerland). The agar pH was measured on solidified agar, at 21 °C, before (pH = 6.4±0.2) and after fungal growth using a flat electrode (Hanna, HI1413B), with a measured uncertainty of 0.01 pH units. Petri dishes containing agar and mica without the fungi were also set up as blanks and incubated together with the inoculated plates.

2.4 Stereomicroscopy

A Leica MZ16 stereoscopic microscope fitted with low temperature fibre optic lighting was used to examine the samples before and after fungal growth. The system was equipped with a digital camera connected to a computer with software that allowed composition of multifocal images (Leica Application Suite, LAS, Leica Microsystems GmbH Wetzlar, Germany).

2.5 Scanning electron microscopy (SEM)-energy dispersive X-ray spectroscopy (EDS)

Phlogopite samples 1-2 cm in diameter were examined uncoated before and after the experiments using a variable pressure SEM (EVO50, Carl Zeiss AG, Germany) equipped with detectors for backscattered electrons (BSE) and secondary electrons (SE). Chemical analysis

was performed by means of EDS (INCA 250, Oxford Instruments). The SEM was fitted with a tungsten filament and operated at 20 keV, with an average working distance of 12.5 mm, and with a chamber pressure between 30 and 150 Pa, chosen according to the need for maintenance of fungal turgidity, and the use of the charge contrast imaging (CCI) operating mode. The CCI mode produces differential surface charge in non-conductive and semi-conductive materials, generating image contrast between areas with compositional or structural differences (Watt *et al.* 2000; Robertson *et al.*, 2005). The EDS analyses were calibrated using standards ($CaCO_3$, SiO_2, Albite, MgO, Al_2O_3, GaP, FeS_2, Wollastonite, MAD-10 Feldspar, Ti and Fe, supplied by Agar Scientific Ltd, Essex, UK) and the conventional ZAF correction (for atomic number Z, absorption and fluorescence) was applied, integrated into the Oxford INCA 250 microanalysis package used.

For the SEM-EDS analysis, the fungal biomass which had colonized the phlogopite was carefully removed, peeling it off with sterile plastic tweezers. In some flakes, however, the fungal biomass was left in place. Where the mineral dissolution was massive (as visually observed), parts of the underlying cellulose layer was also taken for physical support. Some of the EDS analyses were transformed into structural formulas of phyllosilicates (Moore & Reynolds, 1997). Briefly, the chemical composition was recalculated to a half formula unit (anionic charge of 22); all Si and Al up to 4 atoms were assigned to the tetrahedral sheet; the remaining Al, Mg, Fe, Mn and Ti were assigned to the octahedral sheet; and Ca, Na and K were assigned to the interlayer space.

2.6 Statistical analysis

The EDS measurements were analyzed using statistical tests to evaluate the relationships between variables (*e.g.*, measured element, fungal strain, apparent stage of dissolution) and

the significance of the differences between samples and specific areas within each sample. One-way analysis of the variance (ANOVA) was applied, and the significance of the differences was tested at 95% confidence. The ANOVA model used was "unbalanced" because the number of observations within each category was not the same. ANOVA was followed by a post-hoc analysis using Fisher (LSD, Least Significant Difference) and Bonferroni correction procedure in determining the critical value for significance (Sneath & Sokal, 1973).

Statistical analyses of the SEM-EDS chemical data were used to investigate if it was possible to discriminate between weathering mechanisms, whether linked to specific fungi or not. For this, Principal Component Analysis (PCA) and Discriminant Analysis (DA) techniques were applied to the SEM-EDS results in order to establish statistical differences between data obtained from areas of the minerals presenting different degrees of alteration or incubated with different fungal species. PCA was used to study and visualize the correlations between all the variables (Legendre & Legendre, 1998) and to reduce the number of variables for further statistical analysis (Fahmy, 2003; Massart, *et al.*, 1998). The factor scores obtained for the first four principal components (PCs) resulting from PCA were then used to run DA; *i.e.*, the DA analysis was carried out with four variables only (the first four PCs). The step of reducing the number of variables was necessary to run the DA because this analysis requires 3 to 20 times as many samples as variables (Williams & Titus, 1988). ANOVA, PCA and DA analyses were performed using XLSTAT 2009.4.06 software (Addinsoft, Paris, France).

3. Results

3.1 Identification of fungal strains

The pairwise comparison of fungal ITS and bTub sequences with those available in the public online databases confirmed the identity at the species level of *Cladosporium cladosporioides* (Fresen.) G.A. de Vries, and *Alternaria tenuissima* (Kunze) Wiltshire. The *Stilbella* strain could not be identified at the species level using the 5.8S and ITS sequences. *Stilbella* bTub sequence has placed the strain close to the order Hypocreales. The Accession Numbers of the three strains were the following: *Stilbella* sp. (isolate C1) Seq1 KX078478; *C. cladosporioides* (isolate C7) Seq2 KX078479; *A. tenuissima* (isolate F10) Seq3 KX078480; *Stilbella* sp (β-tubulin sequence) KX084402. For brevity, the three fungal isolates are henceforth called *Stilbella, Cladosporium* and *Alternaria*.

3.2 Fungal growth

Alternaria grew well on the mica flakes, covering them partly or entirely under the mycelium (Figure 2a,b). *Stilbella* produced mycelium mainly between the agar and the lower surface of the mica flakes. *Cladosporium* produced an abundant mass of conidia but little mycelium, which grew dispersed on the surface of the mica flakes. The mica flakes showed clear signs of dissolution and became brittle in the experiment with *Alternaria*. Some signs of alteration were observed in the samples inoculated with *Stilbella*. The mica flakes inoculated with *Cladosporium* showed little apparent change. All three fungi showed hyphal adhesion to the surface of mica flakes. The pH of the agar at the beginning of the experiment, before fungal growth, was 6.4±0.2 (at 21 °C). The pH of the agar at the end of the experiment (30-day incubation at 21 °C) was lower for all three species, 5.8±0.3 for *Stilbella,* 5.2± 0.2 for *Cladosporium,* and 4.5± 0.3 for *Alternaria*.

3.3 SEM imaging

Although the degree of growth on the mica flakes was different for each fungus, SEM images revealed that in all cases there was an intimate contact of fungal structures and mica flakes, and that there were signs of alteration in the mica around the points of contact. Figure 3a,b shows SE images of *Stilbella* hyphae (arrows) attached to the phlogopite surface. Both images document the presence of a dark-contrast halo around the hyphae (arrows) indicating an effect of the hyphae on the mica. The contrast is due to differences in surface conductibility that can be observed in the charge contrast imaging (CCI) mode of observation used for these images (Watt *et al.*, 2000). Charge contrast images of SE reveal compositional and/or structural information because both alter charge generation through intracrystalline conductivity (Watt *et al.*, 2000). Thus the contrasted halo around the fungal hyphae (arrows) denotes the presence of a compositional variation of the mica and/or microstructural defects due to fungal attachment. The diffusion of a secreted compound is also compatible with the generation of a charge contrast halo.

Figure 3c (BSE) and 3d (SE) show a branched hypha of *Stilbella*, highlighting the mica sheets forming steps on and near the surface (Figure 3c, BSE) and the surface topography of the flake, the shape of the biological structures and the hyphal adhesion to the mineral (Figure 3d, SE). Figure 3e shows *Cladosporium* hyphae penetrating between mica sheets. Figure 3f shows a detail of a SE image of *Alternaria* hyphae growing on the phlogopite surface where the action of the hypha generated a contrast change.

The SEM BSE signal is strongly dependent on the average atomic number of the specimen. This dependence is the basis for the possibility to discern between chemically different areas in the samples, thus providing a starting point to guide microanalysis in the investigation of the effects of the fungi on phlogopite. *Alternaria* was the species that produced the strongest

changes on mica flakes, with *Stilbella* and *Cladosporium* causing changes that were obvious only in small areas. Thus, we illustrate weathering changes with images from the experiments with *Alternaria.* Figure 4 shows a series of BSE images of mica flakes weathered by *Alternaria* and documents different dissolution mechanisms (compare with the pristine mica surface in Figure 1c). In all the images of Figure 4 the material below the mineral grains is the fungal mass, except in Figure 4e, where the background material is a very thin, corrugated mineral sheet (see below). On occasions, straight and circular troughs developed (Figure 4a) where mica dissolution was more intense, leaving between them less weathered areas of linear and circular shape. More frequently, the mica flakes immersed in the fungal mat were thinned and became almost transparent to the electron beam (Figure 4b,d,e,f). This effect was accompanied by the loss of rigidity of the thin mica flakes, that were bent and folded (Figure 4d,e), and by clear dissolution patterns that reduced the size of the flakes (Figure 4d) or developed as holes within the flakes (Figure 4b,e). Figure 4e and f shows mica flakes thinned and corrugated by fungal weathering with a pattern of contrasting thickness (arrows in Figure 4f) suggesting dissolution of the mineral through contact with or in proximity to the fungal mycelium. On other occasions, dissolution took place more intensely on spots, generating cavities (Figure 4c, arrow 1) on otherwise relatively preserved flakes. Areas of variable contrast were observed on the relatively preserved mica surfaces (Figure 4c). Frequently, but not always, there was a correlation between the contrast and weathering intensity, where more pristine areas had a lighter contrast and more weathered areas had a darker contrast (see below).

The EDS analyses of some of the spots in the images in Figure 4 complement the visual information. The approximate composition of the pristine phlogopite is represented by the spectrum in Figure 1d and spectra b, d and e1 in Figure 4. Spectra b and d are from areas of

light contrast in Figure 4b and 4d, respectively, indicating the differential weathering of the corresponding mica flakes. Spectra in Figure 4e do not show an obvious correlation contrast-chemistry. Spectra e2 and e3 are similar but from areas of different contrast and appearance; whereas spectrum e1 is different but the analysed spot is similar to that where e3 was acquired. The image in Figure 4e is very interesting because it shows two levels of thinning and corrugation of the mica flakes. The top flake is on a corrugated mass of darker contrast. This corrugated mass is very likely a very thin sheet of altered mica placed on the fungal mass. The chemical analysis from this very thin sheet (spectrum e2) is similar to that of areas on the overlying flake (spectrum 3). Other spectra (a1, c1, c2) show clear alteration (obvious decrease of Mg and K, also of Al in c1 and c2) although there is no correlation with the apparent weathering stage. The full description of the EDS data is provided below.

3.4 EDS analysis

From the SEM images, several dissolution stages of phlogopite could be assessed visually and were termed "dense", where the mica flakes preserved a dense appearance with no obvious signs of alteration (Figure 4b and d, spectra b and d); "eroded" where there was erosion of the surface of the flake (arrows in Figure 4a, site 2; 4c, site 1) and/or a darker contrast in the back-scattered SEM images, indicating higher water content (arrows in Figure 4a, site 1; 4d,e,f); and "dissolved", where there was a breakdown of the original flake and groups of small particles remained either within a highly weathered flake (topmost, left area of the mica particle in Figure 4a) or where no large flake remained (Figure 4b, debris within the holes in the mica particle and outside it).

In most EDS analyses of the altered phlogopite, the Si/Fe+Mg+Al ratio increased progressively (Figure 5). Such trend was due to decrease of the octahedral cations Fe and Mg

385 with respect to Si (Figure 5a,c), whereas Al/Si ratio increased for many of the analysed spots
386 (Figure 5b). The interlayer cations also experienced a selective loss, with most analyses
387 showing a lower K+Na+Ca/Si ratio than the original phlogopite (Figure 5d). However, in
388 most cases the only interlayer cation was K, with only a fraction of analyses showing Na and
389 Ca. Potassium was the only interlayer cation in the pristine phlogopite, while Na and Ca were
390 contributed by the nutrient medium. In the control experiments, the surface of the mica
391 appeared fresh and comparable with that of the original mica. Spots of alteration or secondary
392 mineral precipitation had been observed within the circular features of the original mica
393 (Figure 1a,b), which were also observed in the control experiments. These were avoided for
394 the analyses, to ascertain that the evaluation corresponded to weathering taking place in the
395 course of the experiments. The analysis of the surface of the inorganically weathered mica
396 (controls) revealed small departures from the fresh mica surface in which the Si/ Fe+Mg+Al
397 ratio did not vary although Fe/Si increased, Al/Si slightly decreased and Mg/Si decreased
398 (Figure 5). Interestingly, the K/Si ratio increased (no Na or Ca detected in these analyses or in
399 the original mica), indicating a preferential release of Si over K (Figure 5d).
400
401 The alteration of phlogopite in the biological experiments covered a much wider range of
402 chemical changes and progressed much further than in the control experiments. In Figure 5
403 one can observe two groups of data points. The plot in which the two groups were best
404 differentiated was that of Si/ Fe+Mg+Al vs. Al/Si, where the different distribution of data
405 points in both groups was most obvious. The most compact group corresponded to those with
406 a large increase of the Si/ Fe+Mg+Al ratio (in the range 1.58-2.23). In this group there was a
407 coherent arrangement of the data points according to the visual appearance of the analysed
408 grains, where dense, eroded and dissolved grains corresponded to the order of increasing Si/
409 Fe+Mg+Al ratio, or increasing chemical alteration. This group of data points can be described

as generated by an alteration process that resulted in large K loss (low K+Na+Ca/Si; Figure 5d), large Mg loss (low Mg/Si; Figure 5c) and progressive but more reduced Fe and Al loss (Figure 5a,b).

The second group of data points had Si/ Fe+Mg+Al ratios closer to that of the original mica (0.37-1.4) and much wider ranges of Mg/Si, Fe/Si, Al/Si and K+Na+Ca/Si ratios, both above and below those of the original phlogopite. In many cases these ratios were zero, which was rarely observed in the previous group. Thus, the processes generating these weathering products were more chaotic and/or these data included secondary precipitated phases with remains of the weathered mica structure. The only plot that indicated some correlation between the apparent degree of grain alteration (dense, eroded or dissolved) and the chemical trends was that of Si/Fe+Mg+Al vs. Al/Si (Figure 5b). According to it, there was a progressive but widely scattered distribution from dense to eroded and to dissolved mica surface with increasing Al/Si.

The chemical plots included fields that corresponded approximately to the compositions of phlogopite, trioctahedral smectite, dioctahedral smectite, and a line corresponding to kaolinite. These fields allow a rough assessment of whether the weathered mica was transformed into other phyllosilicate phases during the process. The plots in Figure 5 represent a projection of the data on specific planes of the multidimiensional data set. Inspection of the individual projections (each of the plots in Figure 5) informs about the possibility that the data were within specific compositional fields. From Figure 5b,c there were no weathering products within the trioctahedral smectite field. All plots indicated that many of the data points were within the phlogopite field, as expected. Also all plots indicate that many data points were within the dioctahedral smectite field (most probably including the

435 data points in Figure 5c very close to the edge of the dioctahedral smectite field). Finally, the
436 Si/Fe+Mg+Al vs. Fe/Si and Al/Si plots indicated that some data points approached the
437 kaolinite domain (Figure 5a,b). From this analysis, one could hypothesize that during the
438 weathering process a large part of the mica surface experienced a chemical change generating
439 areas and particles of dioctahedral smectite, some of them approaching kaolinitic
440 compositions (high Al, low Mg and Fe). In order to investigate this hypothesis, the individual
441 compositions were tested for a coherent structural formula.
442
443 Approximately half of the chemical analyses on the weathered mica generated coherent
444 structural formulas (Table 1). In these formulas the oxidation state of Fe was assumed from
445 the visual appearance of the mica surface. In surfaces termed "dense", all Fe was assumed to
446 be Fe^{2+}. In all eroded and dissolved grains all Fe was assumed to be Fe^{3+}, as Fe oxidation
447 takes place quickly during weathering. The calculated structural formulas showed the
448 following transition. First, there was a slightly weathered phlogopite, with a decrease of K
449 and octahedral occupancy. These formulas are consistent with the data points in Figure 5
450 within the phlogopite field. Some of these formulas may correspond to vermiculite (interlayer
451 charge 0.6-0.8) which is a typical early alteration product of phlogopite (de la Calle & Suquet,
452 1988). Then, a few structural formulas in which K was further decreased and the octahedral
453 composition was intermediate between dioctahedral and trioctahedral (2.6-2.3). Finally,
454 formulas of a dioctahedral smectite (octahedral occupancy 2.29-1.97) with low K and, in
455 many occasions, with other interlayer cations, such as Na and Ca. These data are consistent
456 with those within the dioctahedral smectite field (Figure 5). Interestingly, no structural
457 formula corresponded to a trioctahedral smectite, confirming also the conclusion from Figure
458 5. From the chemical results, then, it can be concluded that one of the alteration routes of the
459 phlogopite passed through the formation of a dioctahedral smectite of variable Al-Fe-Mg

composition, where Al tends to be the most abundant octahedral cation (Figure 5a,b,c). The weathering process continued with the breakdown of this smectite into phases progressively enriched in Si (Figure 5).

In order to investigate the specific alteration processes promoted by each of the fungus species two chemical plots were considered. First, SEM-EDS data of the fungal mass were collected where the images indicated that no mineral particles were present (Figure 6a). This approach was used to investigate whether some cations were either preferentially assimilated by the fungi or preferentially adsorbed or precipitated on the fungal mycelium. No data exist for *Stilbella* of fungal mass free from mineral particles (no data points for *Stilbella* in Figure 6a). For *Alternaria* and *Cladosporium*, most data points, if not all, were distributed within the ranges found in the analysis of the altered mica flakes (compare Figure 6a with Figure 5d), which suggests that the cation contents in the fungal mass were controlled by very small mineral particles dispersed in the fungal mass not visible with SEM at the range of magnification used. Thus, it was not possible to have information about specific cation assimilation-mobilization by each fungal species. The second approach was to investigate the specific alteration fingerprint that each fungus produced on the mineral particles and surface (Figure 6b; compare with Figure 5d and notice the different key for data points). This approach indicates that *Alternaria* caused alteration in the whole chemical range observed, but most frequently towards decreasing K+Ca+Na/Si, and in many cases there was a substantial increase of the Si/Fe+Mg+Al ratio (Figure 6b). The few *Cladosporium* data mostly showed alteration products where the Si/Fe+Mg+Al ratio remained unchanged and the K+Ca+Na/Si ratio increased. *Stilbella* produced the least aggressive alteration, with little change of Si/Fe+Mg+Al ratios and with K+Ca+Na/Si ratios (most cases meaning K/Si, as there was no Ca or Na) within the phlogopite field or somewhat higher or lower (Figure 6b).

4. Discussion

4.1 Statistical analysis (ANOVA; PCA and correlation; DA between fungi)

PCA was used to investigate the systematic variations between the analysed elements in the dataset in order to obtain a new coordinate system with fewer dimensions (*i.e.*, fewer variables) than the original one. Figure 7a shows the correlation circle obtained on the first two coordinates F1 and F2. Figure 7a is a projection of all the variables on the plane generated by factors F1 and F2. These two new coordinates (principal components, F1 and F2; Figure 7a) explained 64.67% of the total variance of the dataset. According to the plot (Figure 7a) F1 represented the chemical variability between the composition of the organic material (fungal mass, agar nutrient and paper, at the right-hand side of the circle) and phlogopite (left-hand side of the circle). F2 represented the chemical variation between altered phlogopite (top part of the circle) and pristine phlogopite (bottom). Variables (*i.e.*, chemical elements) that are far from the center and close to each other have a significant positive correlation between them (r is positive and high). Variables far from the center and on opposite sides have a significant negative correlation (r is negative and high). Variables at right angles from each other are not correlated (r close to 0). The results are also reported in a more complete but less intuitive fashion in Supplementary data, Table S2, showing the correlation matrix between variables. The major elements in phlogopite (Si, O, Al, Fe, Mg, K) were grouped on the left of the plot and were all strongly and positively correlated (Supplementary data, Table S2; they have p values <0.0001 with a significance level alpha = 0.05). The other elements showed different degrees of correlation, with some significant negative coefficients such as Na and K (p = 0.0046), Cl and Si (p = 0.0003) and Ca and Mg (p<0.0001). Overall, Figure 7a (and Supplementary data, Table S2) indicates the following approximate correlation groups. The elements in the original phlogopite were split by

510 weathering into three groups corresponding to Si-O-Al, Fe, and Mg-K-Ti. Another group was
511 Ca-Na-Mn, where the two first elements were introduced in the system with the PDA nutrient
512 and Mn was a component of the original phlogopite. Phosphorous-Cl-S were another group,
513 all of them from the fungal mass, the PDA nutrient and paper. Carbon had the same origin as
514 this latter group, but appeared isolated from them in the PCA analysis.
515
516 The correlation between K and Mg (Figure 7a) is reasonable because both are nutrients and
517 soluble, which means that they would be selectively removed from the phlogopite flakes.
518 These results are in agreement with previous studies showing Mg and K loss from chlorites
519 and micas (e.g., Leyval & Berthelin, 1991; Paris *et al.*, 1995, 1996; Arocena & Velde, 2009)
520 (Supplementary table 1). The substitution of interlayer K in micas by Na or Ca is also an
521 abiotic process (e.g., Scott & Smith, 1966) but it takes place where the concentration of these
522 cations in the medium is much higher than in our microcosm, which indicates that fungi must
523 have had an active role in the exchange process. Such an active role of the fungi is confirmed
524 by the fact that no Na or Ca exchange occurred in the control experiments. The correlation of
525 Mn with Na and Ca in the PCA may be interpreted as the active translocation by the fungi of
526 solubilized Mn (from dissolved phlogopite areas), Ca and Na (from the nutrient agar) to the
527 interlayer of phlogopite particles in order to extract K. The correlation of Ti with Mg and K in
528 the PCA plot is difficult to explain, as Ti is an immobile element and not a nutrient, as
529 opposed to Mg and K. The position of Fe in the PCA plot is reasonable because Fe is an
530 immobile element but a nutrient, and thus it is expected that the fungi actively mobilized this
531 element, which requires typically the use of siderophores (Chen *et al.*, 2013; Li *et al.* 2016).
532 Finally, the correlation of Si, Al and O is due to the selective removal of the other cations
533 from the phlogopite, because neither Si nor Al are nutrients or soluble. Such relative
534 enrichment in Si and Al by selective depletion of other cations in phyllosilicates during

biological weathering has been reported before (Boyle *et al.* 1967; Paris *et al.*, 1996; Wierzchos & Ascaso, 1996).

Using the PCA analysis, a new system was generated with the principal components (or coordinates) in which the chemical results were investigated in terms of the type of weathering induced by each fungal species. For this, the scores of the chemical values in the new system were analysed using discriminant analysis (DA) to model a set of linearly independent variables capable, if possible, to predict the group to which each variable belongs. Because the principal components (F1, F2,... Fn) are linearly independent by definition, they provide a suitable variable set for group identification. In this experiment, the cumulative variability of the first four components from the PCA analysis accounted for 85.15% of the variance of the whole dataset. Each of these four principal components had eigenvalues above the plateau of the PCA screen plot (not shown), meaning that each one of them was a significant component.

The DA (Figure 7b) showed that the chemical results could be classified according to four categories, which are the three fungal species and the absence of fungal species (controls). In other words, the weathering processes caused by the three fungi on phlogopite could be differentiated from each other and from that of the weathering experiments without fungi. The plot showed two types of complementary results. One is a confidence ellipse for each group. The ellipses are meant to include the maximum number of data points of each group while containing the minimum possible number of results from other groups. The other type of result is the percentage of data (Figure 7b, inset) that were successfully classified into each group (*i.e.*, they fell into the group originally assigned to them) according to the confusing matrix. The most successful classification was that of data from *Alternaria*, followed by the

560 control experiments, *Stilbella* and finally *Cladosporium*.

561

562 Supplementary data, Table S3 reports the average chemical composition of the groups
563 reflecting the different degrees of phlogopite alteration. The significance of the differences
564 between the groups for each element was tested with ANOVA analysis followed by Fisher
565 LSD and Bonferroni tests. The general trend was a statistically significant decrease of the
566 elements Mg, K, Fe, Si and Al from the phlogopite that correlates with the categories "dense",
567 "eroded" and "dissolved", thus confirming a gradual depletion of these elements from the
568 mineral (Figure 8).

569

570 *4.2. Alteration mechanism*

571 It is interesting that the order of increasing weathering effect on phlogopite followed the
572 acidity of the media measured after the experiments, with the values *Alternaria* 4.9±0.3,
573 *Cladosporium* 5.2±0.2 and *Stilbella* 5.8±0.3. This suggests that acid attack was the main
574 mechanism of mica dissolution.

575

576 Our SEM images showed fungal hyphae attached to mica surfaces, and CCI images showed
577 some changes produced on the phlogopite surface by hypha attachment (Figure 3). However,
578 there were no images of later stages of alteration showing weathering patterns that can be
579 related to hyphae distribution on the surface. The CCI images are particularly striking and
580 showed wide areas around the hyphae with a dark contrast (Figure 3a,b,f). Judging by the lack
581 of dissolution features (channels) with a similar shape and distribution perhaps the dark-
582 contrast areas were generated by the diffusion of organic exudates on the mica that did not
583 cause local weathering. An alternative explanation is that fungi produced such an accelerated
584 weathering of lateral progression that the upper mica layer disappeared completely very soon,

obliterating the original channels. We think that the most likely interpretation is that whether or not localized weathering by hyphae took place at an early stage, a more global mechanism of acid attack became more important and dominated the dissolution features.

Balogh-Brunstad *et al.* (2008b) found, in agreement with our results, that experimental biotite dissolution by *Suillus tomentosus* was due predominantly to the exuded organic acids in the bulk liquid, and that immediate hyphal attack of the surface accounted only for 1% of the total dissolution rate. Their experiment was carried out in water, contrary to ours. Other studies show contrasting results. Li *et al.* (2016) found, in experiments with *Talaromyces flavus*, also in water, that the proportion of dissolution caused by hyphal and spore channeling accounted for 40-50% of the dissolved mass. Bonneville *et al.* (2011) investigated the dissolution effect of a single hypha of *Paxillus involutus* on biotite in dry conditions and found that it was significantly faster than the inorganic dissolution of biotite at a pH range 2-4. This study, however cannot be used as a comparison between the effectiveness of microscale (as produced by the hypha) *versus* medium scale dissolution effect of fungi (that might be thought to be represented by the acidic medium of the control). The reason is that fungi do not only exude acidifying substances into the medium as a mechanism of attack but also chelating compounds. Wei *et al.* (2012) imaged with SEM the network of channels created by hyphae of *Aspergillus niger* on muscovite in a medium not saturated with water. The channel network appeared widespread and dense, and seemingly, all signs of corrosion were related to this network. Muscovite, however, is much more resistant to acid degradation than biotite and phlogopite (Kalinowski & Schweda, 1996). It is probable that the combined physico-chemical attack of hyphae (Wei *et al.*, 2012) is more effective than medium-scale chemical attack on the tougher muscovite surfaces, whereas the two mechanisms act similarly on the more labile phlogopite and biotite surfaces. From these results it can be concluded that the mechanism of

610 weathering (hyphal penetration or dissolution of entire grains) depends not only on the level
611 of water saturation (Balogh-Brunstad *et al.*, 2008b) but on many variables that may range
612 from the fungal species to physico-chemical conditions of the fungus-mineral interaction.
613 Natural systems will add also ecological factors to how fungi act and probably introduce a
614 new level of complexity in attack mechanisms. This possibility could be illustrated by the
615 result from Arocena *et al.* (2012), who found that plants inoculated with mycorrhizae were
616 selective in the attack of biotite flakes, leaving some intact, whereas the non-inoculated plants
617 altered all biotite grains. Arocena *et al.* (2012) concluded that this mycorrhizal action could be
618 geared towards a more efficient nutrient extraction that can be sustained longer.
619
620 Figure 5 indicated two types of dissolution of phlogopite. The data points with high
621 Si/Fe+Mg+Al values (1.6 and above) correspond to areas where there was preferential loss of
622 the octahedral cations over Si (apparently similar to the alteration of biotite caused by acidic
623 solutions of inorganic and biological origin described by Boyle *et al.*, 1967). This was the
624 predominant type of alteration that took place in the particle in Figure 4b. The other type of
625 dissolution affected the entire frame of phlogopite and resulted in a more chaotic loss of
626 tetrahedral, octahedral and interlayer cations (Figure 5; Si/Fe+Mg+Al data points at 1.4 and
627 below). This type of dissolution was the most common in the flakes in Figure 4 a,c,d,f. From
628 these results, it appears that none of the two types of weathering just described were
629 recognizable from the morphology of the weathered mica flakes. Further to this, the patterned
630 weathering of the flake in Figure 4a did not produce weathering products different from those
631 in the flakes that were thinned (Figure 4b,d,e,f). The only correlation between chemistry and
632 visual aspect of the weathered mica flakes corresponded to specific areas on the surface of
633 individual flakes, where “dense”, “eroded” and “dissolved” areas generally corresponded to a
634 stage of increased weathering.

635

636 It is of interest to notice that Al was the toughest cation to remove from the phlogopite. This
637 is reasonable considering that (1) Al and Fe are the least soluble among Al, Fe, Mg, K and Si
638 at the pH range measured after the experiments (pH 5-6), and (2) Fe is a micronutrient,
639 whereas Al is not. Cation solubility is highly dependent on the chemistry of the solution and
640 not only linked to pH. It is difficult and beyond the scope of this paper to assess the chemistry
641 at the interface of phlogopite and the solution, where there was the formation of new
642 phyllosilicate phases (Table 1) and possibly of other transient phases of low crystallinity (data
643 points outside the boxes in Figure 5). However, solubility of a cation species at a pH range is
644 a valid starting point to assess the possible mobility of this cation in a weathering process, as
645 we do here. Within the experimental pH range in our study, Al and Fe are the least soluble
646 cations and expected to be mobilized the least from the weathering mica. It is reasonable that
647 the reduced Fe/Al ratios in the weathered substrate were due, at least in part, to selected Fe
648 stabilization in solution and assimilation by the fungi. Siderophore exudation is a specific
649 mechanism of Fe biomobilization and it has been described in *Alternaria* species (Jalal & van
650 der Helm, 1989; Chen *et al.*, 2013). We do not have information about the capacity of the
651 other two fungal species used to exudate siderophores or other highly Fe-selective chelating
652 agents. It cannot be discarded, however, that relative stability conditions of the secondary
653 mineral phases contributed to the reduced Fe/Al ratio in the weathered mica.

654

655 *4.3. Secondary mineral phases*

656 The formation of phyllosilicates of progressively lower layer charge and octahedral content
657 (Table 1) occurred with the three fungi and in all categories of surface weathering stage
658 (dense, eroded and dissolved). However, the number of analyses that produced meaningful
659 phyllosilicate formulas decreased from dense (81% out of 21 analyses) to eroded (56%; 66

analyses) and to dissolved (26%; 31 analyses). Such a result suggests that the formation of the secondary phyllosilicate phases was dominated by the *in situ* transformation of the mica. This would mean that there was cation exchange in the mica and partial crystal reorganization to produce domains in which the octahedral abundance and the layer charge became lower. This is probably supported by an apparent overall decrease of trioctahedral phyllosilicate formulas from dense (35%; 17 analyses) to eroded (51%; 37 analyses) and to dissolved (0%; 6 analyses). These statistical results are less conclusive than the ones above because the number of available analyses was less and the results were more variable. We interpret that the lower percent of trioctahedral formulas for dense surfaces (35%) than for eroded surfaces (51%) is an artifact of the lower sample from the dense surfaces.

Accordingly, our model for this type of weathering in the experiments is that the original phlogopite was transformed into other phases of progressively lower octahedral occupancy (from 3 to 2 atoms per half formula unit) with increasing Al/Fe+Mg and Ca+Na/K ratios. Perhaps, the change from a trioctahedral phase to a dioctahedral phase took place to a greater extent through a dissolution-precipitation mechanism. The control experiments produced weathering products of trioctahedral phyllosilicates of high layer charge, except in one case where the octahedral occupancy was intermediate between trioctahedral and dioctahedral and the layer charge typical of smectite (Table 1). No weathering development was observed by SEM in the controls. Thus, the weathering taking place in the controls was weaker than in the fungal experiments, as ascertained visually and chemically.

About six of the formulas (Table 1) had layer charge 0.6-0.8 per half formula unit and octahedral occupancy definitely trioctahedral (>2.6). These formulas could correspond to vermiculite, which is a typical early alteration product of phlogopite (de la Calle & Suquet,

1988) also when mediated by fungi, free-living (Weed *et al.*, 1969) or in symbiosis (Barker & Banfield, 1996; Wierzchos & Ascaso, 1996; Hinsinger *et al.*, 2006; Arocena *et al.*, 2012). However, many more formulas corresponded to dioctahedral smectite (39), indicating that the possible vermiculite stage was transient or rare. This type of weathering, in which phlogopite or biotite are transformed into dioctahedral phyllosilicate phases, has been observed driven by inorganic causes in other studies. Such is the case of phlogopite alteration to beidellite (dioctahedral, Al-rich smectite), with lateral continuity of layers between pristine and weathered domains, caused by intense weathering in a karstic environment (Aldega *et al.*, 2009). Similarly, Aoudjit *et al.* (1995) reported trioctahedral micas altered to beidellite in well-drained granitic saprolites in a humid climate, with mildly acidic pH (~6.5), and Ahn & Peacor (1987) reported the transformation of biotite into kaolinite under high CO_2 activity, and thus perhaps also under somehow acidic conditions. Thus, the type of weathering that produced phyllosilicates of different composition in our experiments is not exclusive of fungal action. In our case, however, these transformations took place in 30 days, rather than in the much more extended periods that can be assumed for the above examples (~840 ky in the case of Aldega *et al.*, 2009). The much faster rate in our experiments was due to the large fungal development, the aggressive action driven by fungal metabolism and possibly lower pH values. Phlogopite fast weathering at low pH is well documented (*e.g.*, Kuwahara & Aoki, 1995).

Considering that the number of meaningful phyllosilicate formulas decreased constantly from areas labelled as dense to eroded and to dissolved, it is most likely that the dioctahedral smectite was also a transient phase in our experiments, that progressed towards dissolution. Kaolinite is the most stable dioctahedral phyllosilicate in acidic environments (Garrels & Christ, 1965) but no analytical data appeared in the kaolinite field (a line in Figure 5a,b). This

may be one more reason to consider that the predominant mechanism in the formation of the phyllosilicate phases was cation exchange and partial rearrangement of the atoms rather than dissolution and precipitation, which should have produced kaolinite according to the pH conditions in our experiments.

5. Conclusions

Our study shows that, in controlled studies, it is possible to recognize the alteration footprint of individual fungal species on individual minerals. This is valuable information and indicates the potential of relating chemical weathering features to types of fungi in nature. However, the fungal footprint may well change in natural environments due to the diversity of microbial community, available mineral sources, mineral particle size and water regime, just to cite some of the most evident variables. The experiment was based on a system in vitro maintained at 100% relative humidity that did not simulate the heterogeneity of natural terrestrial or rock surface environments, but aimed at controlling variables. It will be interesting to test the possibility of discerning specific weathering footprints in experiments of increasing complexity. This line of research would have two goals, (1) to study the possibility of identifying the past or present presence of specific fungal groups by their weathering footprint, and (2) to investigate how this footprint may vary with changing variables and thus indicate the changes in fungal strategies to obtain mineral nutrients.

The experiments in our study represent systems where the fungal aggression to the mineral particles was high (with large fungal mass development and enveloping of the mineral grains). In this situation, about half of the weathered phlogopite areas analysed had a chemical composition consistent with phyllosilicates with a trend towards Al-rich (dioctahedral) smectite. The other half of the analysed areas corresponded to non-phyllosilicate phases,

735 probably the residue of dissolution or mixed precipitated silicate and salt phases. Arguably, in
736 natural systems, the fungal aggression to individual mineral grains is less intense, because the
737 system is open and there is a less concentrated fungal development on mineral grains. In such
738 a system it is plausible that the alteration of mica flakes proceeds to a lesser extent, or more
739 slowly, than in our experiments and that Al-rich clay is a more abundant product. Thus, our
740 results are in agreement with fungal action as an effective modifier of mica grains into
741 expandable clays, much faster than inorganic agents (our experiments lasted 30 days). Part of
742 the very degraded silicate material formed by intense leaching can react towards the formation
743 Al-rich clay, smectite or kaolinite, after the direct biological action on the grain ceases. The
744 reasons are that (1) these degraded silicate phases are probably very reactive and (2) Al-
745 smectite and kaolinite are the most stable silicate mineral phases in pedogenic environments
746 (Weaver, 1989). Thus, fungal activity may promote Al-rich clay formation through direct and
747 indirect routes.

748

749 **Acknowledgments**

750 The comments and criticism of two anonymous reviewers helped to inprove the manuscript.

751

752 **Conflict of interest**

753 The authors have no conflict of interest to declare.

754

755 **References**

756 Abarenkov K, Nilsson RH, Larsson K-H, Alexander IJ, Eberhardt U, Erland S, Hoiland K,
757 Kjoller R, Larsson E, Pennanen T, Sen R, Taylor AFS, Tedersoo L, Ursing BM,
758 Vralstad T, Liimatainen K, Peintner U, Koljalg U, 2010. The UNITE database for
759 molecular identification of fungi - recent updates and future perspectives. *New*
760 *Phytologist* **186**: 281-285.
761 Adeyemi AO, Gadd GM, 2005. Fungal degradation of calcium-, lead- and silicon-bearing
762 minerals. *BioMetals* **18**: 269-281.

763 Ahn JH, Peacor DR, 1987. Kaolinization of biotite: TEM data and implications for an
764 alteration mechanism. *American Mineralogist* **72**: 353-356.
765 Aldega L, Cuadros J, Laurora A, Rossi A, 2009. Weathering of phlogopite to beidellite in a
766 karstic environment. *American Journal of Science* **309**: 689-710.
767 Altschul SF, Madden TL, Schäffer AA, Zhang J, Zhang Z, Miller W, Lipman JD, 1997.
768 Gapped BLAST and PSI-BLAST: a new generation of protein database search
769 programs. *Nucleic Acids Research* **25**: 3389-3402.
770 Aoudjit H, Robert M, Elsass F, Curmi P, 1995. Detailed study of smectite genesis in granitic
771 saprolites by analytical electron microscopy. *Clay Minerals* **30**: 135-147.
772 Arocena JM, Velde B, 2009. Transformation of chlorites by primary biological agents - a
773 synthesis of X-ray diffraction studies. *Geomicrobiology Journal* **26**: 382-388.
774 Arocena JM, Velde B, Robertson SJ, 2012. Weathering of biotite in the presence of
775 arbuscular mycorrhizae in selected agricultural crops. *Applied Clay Science* **64**: 12-17
776 Arvieu J-C, Leprince F, Plassard C, 2003. Release of oxalate and protons by ectomycorrhizal
777 fungi in response to P deficiency and calcium carbonate in nutrient solution. *Annals of*
778 *Forest Science* **60**: 209-215.
779 Balogh-Brunstad Z, Keller CK, Bormann BT, O'Brien R, Wang D, Hawley G, 2008a.
780 Chemical weathering and chemical denudation dynamics through ecosystem
781 development and disturbance. *Global Biogeochemical Cycles* **22**: GB1007.
782 doi:10.1029/2007GB002957.
783 Balogh-Brunstad Z, Keller CK, Dickinson JT, Stevens F, Li CY, Bormann BT, 2008b. Biotite
784 weathering and nutrient uptake by ectomycorrhizal fungus, *Suillus tomentosus*, in
785 liquid-culture experiments. *Geochimica et Cosmochimica Acta* **72**: 2601-2618.
786 Banfield JF, Barker WW, Welch SA, Taunton A, 1999. Biological impact on mineral
787 dissolution: application of the lichen model to understanding mineral weathering in the
788 rhizosphere. *Proceedings of the National Academy of Sciences of the United States of*
789 *America* **96**: 3404-3411.
790 Barker WW, Banfield JF, 1996. Biologically versus inorganically mediated weathering
791 reactions: relationships between minerals and extracellular microbial polymers in
792 lithobiontic communities. *Chemical Geology* **132**: 55-69.
793 Barker WW, Welch SA, Banfield JF, 1997. Biogeochemical weathering of silicate minerals.
794 *Reviews in Mineralogy and Geochemistry* **35**: 391-428.
795 Blum JD, Klaue A, Nezat CA, Driscoll CT, Johnson CE, Siccama TG, Eagar C, Fahey TJ,
796 Likens GE, 2002. Mycorrhizal weathering of apatite as an important calcium source in
797 base-poor forest ecosystems. *Nature* **417**: 729-731.
798 Bonneville S, Morgan DJ, Schmalenberger A, Bray A, Brown A, Banwart SA, Benning LG,
799 2011. Tree-mycorrhiza symbiosis accelerate mineral weathering: Evidences from
800 nanometer-scale elemental fluxes at the hypha-mineral interface. *Geochimica et*
801 *Cosmochimica Acta* **75**: 6988-7005.
802 Bonneville S, Smits MM, Brown A, Harrington J, Leake JR, Brydson R, Benning LG, 2009.
803 Plant-driven fungal weathering: Early stages of mineral alteration at the nanometer
804 scale. *Geology* **37**: 615-618.
805 Boyle JR, Voigt GK 1973 Biological weathering of silicate minerals, implications for tree
806 nutrition and soil genesis. *Plant Soil* **38**: 191-201.
807 Boyle JR,Voigt GK, Sawhney BL, 1967. Biotite flakes: alteration by chemical and biological
808 treatment. *Science* **155**: 193-195.
809 Bray AW, Oelkers EH, Bonneville S, Wolff-Boenisch D, Potts NJ, Fones G, Benning LG,
810 2015. The effect of pH, grain size, and organic ligands on biotite weathering rates.
811 *Geochimica et Cosmochimica Acta* **164**: 127-145.

812 Burford EP, Fomina M, Gadd GM 2003a Fungal involvement in bioweathering and
813 biotransformation of rocks and minerals. *Mineralogical Magazine* **67**: 1127-1155.
814 Burford EP, Kierans M., Gadd GM, 2003b. *Geomycology: fungi in mineral substrata.*
815 Mycologist, Volume 17, Part 3 August. Cambridge University Press Printed in the
816 United Kingdom. DOI: 10.1017/S0269915X03003112
817 Burford EP, Hillier S, Gadd GM, 2006. Biomineralization of fungal hyphae with calcite
818 ($CaCO_3$) and calcium oxalate mono- and dihydrate in carboniferous limestone
819 microcosms. *Geomicrobiology Journal* **23**: 599-611.
820 Burgstaller W, Schinner F, 1993. Leaching of metals with fungi. *Journal of Biotechnology* **27**:
821 91-116.
822 Chen L-H, Lin C-H, Chung K-R, 2013. A non ribosomal peptide synthetase mediates
823 siderophore production and virulence in the citrus fungal pathogen *Alternaria alternata*.
824 *Molecular Plant Pathology* **14**: 497-505.
825 Costa A, Chiodini G, Granieri D, Folch A, Caliro S, Avino R, Cardellini C 2008 A shallow-
826 layer model for heavy gas dispersion from natural sources: Application and hazard
827 assessment at Caldara di Manziana, Italy. *Geochemistry, Geophysics, Geosystems* **9**:
828 Q03002, doi: 10.1029/2007GC001762.
829 Crawford RH, Floyed M, Li CY, 2000. Degradation of serpentine and muscovite rock
830 minerals and immobilization of cations by soil *Penicillium* spp. *Phyton-annales rei*
831 *botanicae* **40**: 315-322.
832 Cuadros J, Afsin B, Jadubansa P, Ardakani M, Ascaso C, Wierzchos J, 2013. Microbial and
833 inorganic control on the composition of clay from volcanic glass alteration experiments.
834 *American Mineralogist* **98**: 319-334.
835 de la Calle, C, Suquet, H, 1988. Vermiculite. In: Bailey SW (ed), *Hydrous Phyllosilicates*
836 *(exclusive of micas)*, Vol 19, Mineralogical Society of America, Washington, DC, pp.
837 455-496.
838 Driessen P, Deckers J, Spaargaren O, Nachtergaele F, 2001. *Lecture notes on the major soils*
839 *of the world*. FAO, Rome, ISBN 925-104637-9.
840 Fahmy T 2003 *XLSTAT-Pro 7.0* (XLSTAT), Addinsoft. Paris, France.
841 Fomina M, Burford EP, Gadd GM, 2006. Fungal dissolution and transformation of minerals:
842 significance for nutrient and metal mobility. In: Gadd GM (ed), *Fungi in*
843 *Biogeochemical Cycles*, Cambridge University Press, Cambridge, MA, pp. 236-266.
844 Fomina M, Hillier S, Charnock JM, Melville K, Alexander IJ, Gadd GM, 2005. Role of oxalic
845 acid over-excretion in toxic metal mineral transformations by *Beauveria caledonica*.
846 *Applied Environmental Microbiology* **71**: 371-381.
847 Fomina M., Podgorsky VS, Olishevska SV, Kadoshnikov VM, Pisanska IR, Hillier S, Gadd
848 GM, 2007. Fungal Deterioration of Barrier Concrete used in Nuclear Waste Disposal.
849 *Geomicrobiology Journal* **24**: 643-653.
850 Foster MS, Bills GF 2011 Biodiversity of Fungi: Inventory and Monitoring Methods, Elsevier
851 Academic Press, USA, 777 pp.
852 Gadd GM, 1999. Fungal production of citric and oxalic acid: importance in metal speciation,
853 physiology and biogeochemical processes. *Advances in Microbial Physiology* **41**: 47-
854 92.
855 Gadd GM, Sayer JA, 2000. Fungal transformations of metals and metalloids. In: Lovley DR
856 (ed), *Environmental Microbe–Metal Interactions*, American Society for Microbiology,
857 Washington, DC, pp. 237-256.
858 Garrels RM, Christ CL, 1965. *Solutions, Minerals, and Equilibria*. Harper and Row, New
859 York. 450 pp.
860 Gazzè SA, Saccone L, Ragnarsdottir KV, Smits MM, Duran A. L., Leake JR, Banwart SA,
861 McMaster TJ, 2012. Nanoscale channels on ectomycorrhizal-colonized chlorite:

Evidence for plant-driven fungal dissolution. *Journal of Geophysical Research* **117**: G00N09, doi:10.1029/2012JG002016.

Glass NL, Donaldson GC, 1995. Development of primer sets designed for use with the PCR to amplify conserved genes from filamentous ascomycetes. *Applied and Environmental Microbiology* **61**: 1323-1330.

Gleeson DB, Clipson NJW, Melville K, Gadd GM, McDermott FP, 2005. Mineralogical control of fungal community structure in a weathered pegmatitic granite. *Microbial Ecology* **50**: 360-368.

Hansel CM, Zeiner CA, Santelli CM, Webb SM, 2012. Mn(II) oxidation by an ascomycete fungus is linked to superoxide production during asexual reproduction. *Proceedings of the National Academy of Sciences of the United States of America* **109**: 12621-12625.

Hinsinger P, Plassard C, Jaillard B, 2006. Rhizosphere: a new frontier for soil biogeochemistry. *Journal of Geochemical Exploration* **88**: 210-213.

Hoffland E, Kuyper TW, Wallander H, Plassard C, Gorbushina AA, Haselwandter K, Holmström S, Landeweert R, Lundström US, Rosling A, Sen R, Smits MM, van Hees PAW, van Breemen N, 2004. The role of fungi in weathering. *Frontiers in Ecology and the Environment* **2**: 258-264.

Hoffland E, Smits MM, Van Schöll L, Landeweert, R, 2005. Rock-eating mycorrhizas: mobilizing nutrients from minerals? In: Li CJ, Zhang FS, Doberman A, Hinsinger P, Lambers H, Li XL, Marschner P, Maene L, McGrath S, Oenema O, Peng SB, Rengel Z, Shen QR., Welch R, Von Wirén N, Yan XL, Zhu YG (eds), *Plant nutrition for food security, human health and environmental protection*, Beijing, pp 802-803.

Hopf J, Langenhorst F, Pollok K, Merten D, Kothe E, 2009. Influence of microorganisms on biotite dissolution: An experimental approach. *Chemie Der Erde-Geochemistry* **69**: 45-56. doi:10.1016/j.chemer.2008.11.001.

Jalal MA, van der Helm D, 1989. Siderophores of highly phytopathogenic *Alternaria longipes*. Structures of hydroxycoprogens. *BioMetals* **2**: 11-17.

Jenny H, 1980. The *Soil Resource: Origin and Behavior*. Springer-Verlag, New York.

Jongmans AG, vanBreemen N, Lundström U, vanHees PAW, Finlay RD, Srinivasan M, Unestam T, Giesler R, Melkerud P-A, Olsson M, 1997. Rock-eating fungi. *Nature* **389**: 682-683. doi:10.1038/39493.

Kalinowski BE, Schweda P, 1996. Kinetics of muscovite, phlogopite, and biotite dissolution and alteration at pH 1-4, room temperature. *Geochimica et Cosmochimica Acta* **60**: 367-385. doi:10.1016/0016-7037(95)00411-4.

Karsch-Mizrachi I, Nakamura Y, Cochrane G, 2012. The International Nucleotide Sequence Database Collaboration. *Nucleic Acids Research* **40**: D33-D37.

Kõljalg U, Larsson KH, Abarenkov K, Nilsson RH, Alexander IJ, Eberhardt U, Erland S, Høiland K, Kjøller R, Larsson E, Pennanen T, Sen R, Taylor AF, Tedersoo L, Vrålstad T, Ursing BM, 2005. UNITE: a database providing web-based methods for the molecular identification of ectomycorrhizal fungi. *New Phytologist* **166**: 1063-1068.

Kuwahara Y, Aoki Y, 1995. Dissolution process of phlogopite in acid solutions. *Clays and Clay Minerals* **43**: 39-50.

Legendre P, Legendre L, 1998. Numerical Ecology, second Ed. Amsterdam, Elsevier.

Leyval C, Berthelin J, 1991. Weathering of mica by roots and rhizospheric microorganisms of pine. *Soil Science Society of America Journal* **55**: 1009-1016.

Li Z, Liu L, Chen J, Teng HH, 2016. Cellular dissolution at hypha- and spore-mineral interfaces revealing unrecognized mechanisms and scales of fungal weathering. *Geology*, G37561.1. doi:10.1130/G37561.1

Lou J, Fu L, Peng Y, Zhou L, 2013. Metabolites from *Alternaria* Fungi and Their Bioactivities. *Molecules* **18**: 5891-5935.

912 Mackenzie RC (1970) *Differential Thermal Analysis*, London, Academic Press.
913 Massart DL, Vandeginste BGM, Buydens LMC, de Jong S, Lewi PJ, Smeyers Verbeke J,
914 1998. *Handbook of Chemometrics and Qualimetrics*. Part B. Elsevier Science,
915 Amsterdam.
916 Moore DM, Reynolds RC Jr, 1997. *X-ray Diffraction and the Identification and Analysis of*
917 *Clay Minerals*. 2nd edition. Oxford University Press, Oxford. 378 pp.
918 Paris F, Bonnaud P, Ranger J, Lapeyrie F, 1995. In vitro weathering of phlogopite by
919 ectomycorrhizal fungi: 1. Effect of K^+ and Mg^{2+} deficiency on phyllosilicate evolution.
920 *Plant & Soil* **177**: 191-201. doi:10.1007/BF00010125.
921 Paris F, Botton B, Lapeyrie F, 1996. In vitro weathering of phlogopite by ectomycorrhizal
922 fungi. II. Effect of K^+ and Mg^{2+} deficiency and N sources on accumulation of oxalate
923 and H^+. *Plant & Soil* **179**: 141-150.
924 Robertson K, Gauvin R, Finch J, 2005. Application of charge contrast imaging in mineral
925 characterization. *Minerals Engineering* **18**: 343-352.
926 Rosling A, Lindahl BD, Finlay RD, 2004a. Carbon allocation to ectomycorrhizal roots and
927 mycelium colonising different mineral substrates. *New Phytologist* **162**, 795-802.
928 Rosling A, Lindahl BD, Taylor AFS, Finlay RD, 2004b. Mycelial growth and substrate
929 acidification of ectomycorrhizal fungi in response to different minerals. *FEMS*
930 *Microbiology Ecology* **47**: 31-37.
931 Rosling A, Suttle KB, Johansson E, Van Hees PAW, Banfield JF, 2007. Phosphorous
932 availability influences the dissolution of apatite by soil fungi. *Geobiology* **5**: 265-280.
933 Saccone L, Gazze SA, Ragnarsdottir KV, Leake JR, Duran AL, Hallam KR, Mcmaster TJ,
934 2009. *Paxillus involutus* hyphae: imaging their structure and interaction with mineral
935 surfaces using AFM. *Geochimica et Cosmochimica Acta* **73**: A1140.
936 Scott AD, Smith SJ,. 1966. Susceptibility of interlayer potassium in micas to exchange with
937 sodium. *Clays Clay Mineral* **14:** 69-81
938 Sneath PHA, Sokal RR, 1973. Numerical Taxonomy. Freeman, San Francisco, USA.
939 Sterflinger K, 2000. Fungi as geologic agents. *Geomicrobiology Journal* **17**: 97-124.
940 Thomas P, 2012. Long-term survival of *Bacillus* spores in alcohol and identification of 90%
941 ethanol as relatively more spori/bactericidal. *Current Microbiology* **64**, 130-139.
942 Wallander H, 2006. Mineral dissolution by ectomycorrhizal fungi. In: Gadd GM (ed), *Fungi*
943 *in Biogeochemical Cycles*, Cambridge University Press, New York, NY, pp. 328-343.
944 Wallander H, Wickman T, 1999. Biotite and microcline as potassium sources in
945 ectomycorrhizal and non-ectomycorrhizal *Pinus sylvestris* seedlings. *Mycorrhiza* **9**: 25-
946 32.
947 Watt GR, Griffin B, Kinny P, 2000. Charge contrast imaging of geological materials in the
948 environmental scanning electron microscope. *American Mineralogist* **85**: 1784-1794.
949 Weaver CE, 1989. *Clays, Muds, and Shales*. Developments in Sedimentology v. 44, Elsevier,
950 Amsterdam.
951 Weed SB, Davey CB, Cook MG, 1969. Weathering of mica by fungi. *Soil Science Society of*
952 *America Proceedings* **33**: 702-706.
953 Wei Z, Kierans M, Gadd GM, 2012. A model sheet mineral system to study fungal
954 bioweathering of mica. *Geomicrobiology Journal* **29**: 323-331.
955 Welch SA, Vandevivere P 1994 Effect of microbial and other naturally occurring polymers on
956 mineral dissolution. *Geomicrobiology Journal* **12**: 227-238.
957 White TJ, Bruns T, Lee S, Taylor J, 1990. Amplification and direct sequencing of fungal
958 ribosomal RNA genes for phylogenetics. In: Innis MA, Gelfand DH, Sninsky JJ, White
959 TJ (eds), *PCR Protocols: a guide to methods and applications*, Academic Press, New
960 York, USA, pp. 315-322.

961 Wierzchos J, Ascaso C, 1996. Morphological and chemical features of bioweathered granitic
962 biotite induced by lichen activity. *Clays and Clay Minerals* **44**: 652-657.
963 Williams BK, Titus K 1988 Assessment of sampling stability in ecological applications of
964 discriminant analysis. *Ecology* **69**: 1275-1285.
965 Yuan L, Huang JG, Li XL, Christie P, 2004. Biological mobilization of potassium from clay
966 minerals by ectomycorrhizal fungi and eucalypt seedling roots. *Plant & Soil* **262**: 351-
967 361.

Figure captions

Figure 1. a) and b) Stereomicroscope images of the original phlogopite at two magnifications. The circular structures are of unknown origin but most probably due to inclusions. c) VP-SEM backscattered electron image of the surface of a pristine phlogopite flake; d) EDS spectrum from the surface in c).

Figure 2. a) *Alternaria* colonies developing close and on phlogopite flakes (two flakes are completely covered on both sides of the visible flake) in the agar-cellulose microcosm (view from above the Petri dish). b) Stereomicroscope image of *Alternaria* hyphae growing on a phlogopite flake. c) *Stilbella* colonies developing under a phlogopite flake in the agar-cellulose microcosm (view from below the Petri dish). d) Stereomicroscope image of *Stilbella* hyphae growing on phlogopite. e) *Cladosporium* colonies developing on a phlogopite flake in the agar-cellulose microcosm (view from above the Petri dish); f) Stereomicroscope image of *Cladosporium* hyphae growing on a phlogopite flake.

Figure 3. VP-SEM images of mica flakes and fungal mass. a) Secondary electrons (SE) image in charge contrast imaging mode (CCI) at 47 Pa of *Stilbella* hyphae (arrows) growing on phlogopite surface. The hyphae produced changes in the mica surface that generated a dark-contrast halo around the hyphae (see text). b) SE image in CCI mode of *Stilbella* hyphae and clusters of cells developing on phlogopite surface with the dark halo around them (arrows). c) Backscattered electrons (BSE) image of a *Stilbella* hypha growing on the phlogopite; the sheet morphology of the mica is revealed. d) The same image (c) observed with the SE detector, which highlights the surface topography and hyphal adhesion to the mineral. e) BSE image of *Cladosporium* hyphae penetrating between the sheets of the mineral. f) SE image in CCI mode at 50 Pa of *Alternaria*

hyphae growing on phlogopite surface, showing the detail of the halo around the hyphae probably induced by fungal activity; the black arrow shows the point of contrast change on the mica surface and the white arrow the location of one of the hyphae.

Figure 4. VP-SEM backscattered electrons (BSE) images of phlogopite mineral samples weathered by *Alternaria*. a) Differential dissolution produces circular (arrow 1) and linear (arrow 2) grooves with more dense areas between them. The EDS spectrum from the spot indicated by arrow 1 is spectrum a1 below. b) Phlogopite flake immersed in fungal mat, thinned, and made almost transparent to the electron beam by weathering. EDS spectrum b is from the spot indicated by the arrow and indicates a close-to-pristine composition. c) Detail of the surface of a flake with a cavity apparently produced by dissolution (arrow 1) and areas of apparent pristine density (arrow 2). However, EDS spectra c1 and c2 (arrows) reveal the similar composition of both spots. d) Mica sheet partly dissolved by the fungal action with areas of different degree of weathering. EDS spectrum d indicates little weathering effect in the corresponding spot (arrow). e) Mica sheet that has been thinned and corrugated, with different degrees of weathering (EDS spectra e1 and e3). This mica sheet is on a mass of more severely corrugated mica (EDS spectrum e2). f) Part of a mica sheet with areas of different thickness (arrows).

Figure 5. Chemical plots from SEM-EDS analyses of the mineral alteration products. The chemical ratios were chosen to provide a view of relative chemical variations of the octahedral (a, b, c) and interlayer (d) cations, with respect to Si. The key to the symbols is provided in (a). The boxes represent approximate compositional fields of the mineral phases indicated in (a). Control experiments correspond to alteration in absence of

fungi. Dense, eroded and dissolved correspond to apparent stages of mica weathering in the experiments with the fungi (see text).

Figure 6. Chemical plots from SEM-EDS analyses of the fungal mass (a) and the mineral alteration products from each fungal species (b). The key to the symbols is provided in (a). The boxes are defined in Figure 5.

Figure 7. Statistical analyses of the chemical SEM-EDS results from the weathered phlogopite. a) Principal Component Analysis (PCA) projected on the first two coordinates F1 and F2, with the corresponding % of variability of the data that each of them explains. The plot indicates correlations between chemical elements (proximity between them and location far from the centre of the plot). b) Discriminant Analysis (DA) plot. The axes are represented with the corresponding % of data variability that they explain. The DA model shows that the chemical results can be classified according to four categories, the three fungal species and the lack of fungal species (controls). The ellipses represent the categories found by the DA model. The percent of data that have been correctly classified as pertaining to each specific category are reported (inset).

Figure 8. Average atomic % contents from multiple SEM-EDS analyses of the several substrates (or categories): "mica" is the unaltered mineral; "dense", "eroded" and "dissolved" correspond to the mineral in a progressive weathering stage; “fungus” is the fungal mass (although it was observed that EDS analysis of fungal mass corresponded to minute mineral grains; see text). Error bars are the standard deviation values.

Table 1

Table 1. Structural formulas (half formula unit) of alteration products calculated from SEM-EDS analyses.

	Si	Al^{IV}	Al^{VI}	Mg	Fe^{3+}	Fe^{2+}	Mn	Ti	Ca	Na	K	Sum oct.	Int. charge
Orig. mica	2.75	1.25	0.14	2.09	0.00	0.49	0.00	0.17	0.00	0.00	0.98	2.89	0.98
Control	2.73	1.27	0.04	2.08	0.00	0.71	0.00	0.16	0.00	0.00	0.93	2.99	0.93
Control	2.78	1.22	0.05	2.22	0.00	0.47	0.00	0.17	0.00	0.00	0.99	2.91	0.99
Control	2.79	1.21	0.04	2.23	0.00	0.48	0.00	0.17	0.00	0.00	1.00	2.91	1.00
Control	2.81	1.19	0.13	2.10	0.00	0.51	0.00	0.15	0.00	0.00	0.97	2.89	0.97
Control	3.21	0.79	1.08	0.79	0.00	0.57	0.00	0.08	0.00	0.00	0.49	2.52	0.49
Alternaria	2.73	1.27	0.09	2.28	0.00	0.47	0.00	0.15	0.00	0.00	0.91	2.99	0.91
Alternaria	2.75	1.25	0.12	2.27	0.00	0.45	0.00	0.14	0.00	0.00	0.88	2.98	0.88
Alternaria	2.82	1.18	0.21	2.36	0.39	0.00	0.00	0.00	0.00	0.00	0.69	2.95	0.69
Alternaria	2.81	1.19	0.63	2.31	0.00	0.00	0.00	0.00	0.00	0.00	0.68	2.94	0.68
Alternaria	2.82	1.18	0.22	2.35	0.36	0.00	0.00	0.00	0.00	0.00	0.73	2.94	0.73
Alternaria	2.64	1.36	0.06	2.32	0.40	0.00	0.00	0.12	0.06	0.00	0.73	2.90	0.85
Alternaria	2.78	1.22	0.54	2.36	0.00	0.00	0.00	0.00	0.00	0.00	0.89	2.90	0.89
Alternaria	2.76	1.24	0.32	2.09	0.47	0.00	0.00	0.00	0.00	0.00	0.69	2.88	0.69
Stilbella	2.95	1.05	0.22	2.00	0.00	0.45	0.00	0.14	0.00	0.00	0.90	2.82	0.90
Stilbella	2.67	1.33	0.03	2.17	0.47	0.00	0.00	0.14	0.00	0.00	0.91	2.82	0.91
Stilbella	2.99	1.01	0.22	2.01	0.00	0.43	0.00	0.14	0.00	0.00	0.89	2.80	0.89
Stilbella	2.97	1.03	0.23	1.97	0.00	0.44	0.00	0.15	0.00	0.00	0.90	2.80	0.90
Stilbella	2.68	1.32	0.08	2.09	0.47	0.00	0.00	0.16	0.00	0.00	0.87	2.79	0.87
Stilbella	2.73	1.27	0.03	2.08	0.50	0.00	0.00	0.16	0.00	0.00	0.89	2.77	0.89
Stilbella	2.72	1.28	0.06	2.08	0.48	0.00	0.00	0.15	0.00	0.00	0.89	2.77	0.89
Stilbella	2.71	1.29	0.08	2.08	0.44	0.00	0.00	0.15	0.00	0.00	0.96	2.75	0.96
Cladosporium	2.87	1.13	0.43	1.62	0.00	0.56	0.00	0.14	0.00	0.00	0.91	2.75	0.91
Alternaria	2.73	1.27	0.14	1.79	0.81	0.00	0.00	0.00	0.00	0.00	0.83	2.74	0.83
Stilbella	2.75	1.25	0.07	2.02	0.48	0.00	0.00	0.16	0.00	0.00	0.91	2.73	0.91
Stilbella	2.81	1.19	0.34	1.83	0.42	0.00	0.00	0.13	0.00	0.00	0.73	2.72	0.73
Stilbella	2.77	1.23	0.07	1.98	0.50	0.00	0.00	0.15	0.00	0.00	0.93	2.71	0.93
Cladosporium	2.78	1.22	0.22	1.82	0.49	0.00	0.00	0.15	0.00	0.00	0.86	2.68	0.86
Stilbella	2.85	1.15	0.46	1.60	0.50	0.00	0.00	0.11	0.00	0.00	0.63	2.67	0.63
Alternaria	2.75	1.25	0.38	1.77	0.42	0.00	0.00	0.08	0.08	0.10	0.70	2.66	0.96
Stilbella	2.98	1.02	0.19	1.82	0.47	0.00	0.00	0.14	0.00	0.00	0.82	2.63	0.82
Cladosporium	2.82	1.18	0.24	1.70	0.54	0.00	0.00	0.15	0.00	0.00	0.86	2.63	0.86
Stilbella	2.99	1.01	0.20	1.82	0.46	0.00	0.00	0.15	0.00	0.00	0.82	2.62	0.82
Stilbella	2.97	1.03	0.17	1.86	0.44	0.00	0.00	0.14	0.00	0.00	0.89	2.62	0.89
Stilbella	2.80	1.20	0.31	1.65	0.50	0.00	0.00	0.15	0.00	0.00	0.85	2.62	0.85
Stilbella	2.98	1.02	0.15	1.84	0.46	0.00	0.00	0.15	0.00	0.00	0.92	2.60	0.92
Stilbella	2.96	1.04	0.10	1.84	0.47	0.00	0.00	0.17	0.00	0.00	0.95	2.59	0.95
Stilbella	2.88	1.12	0.52	1.44	0.48	0.00	0.00	0.13	0.00	0.00	0.73	2.57	0.73
Stilbella	2.89	1.11	0.74	1.21	0.46	0.00	0.00	0.12	0.00	0.00	0.61	2.53	0.61
Stilbella	2.93	1.07	0.73	1.20	0.48	0.00	0.00	0.11	0.00	0.00	0.61	2.52	0.61
Stilbella	2.92	1.08	0.76	1.16	0.48	0.00	0.00	0.11	0.00	0.00	0.60	2.51	0.60
Stilbella	3.17	0.83	0.42	1.66	0.42	0.00	0.00	0.00	0.00	0.00	0.99	2.50	0.99
Stilbella	3.03	0.97	0.63	1.22	0.54	0.00	0.00	0.11	0.00	0.00	0.60	2.49	0.60
Stilbella	2.96	1.04	0.81	1.11	0.49	0.00	0.00	0.09	0.00	0.00	0.58	2.49	0.58
Stilbella	2.94	1.06	1.10	0.92	0.39	0.00	0.00	0.07	0.00	0.00	0.47	2.48	0.47
Stilbella	2.98	1.02	1.13	0.91	0.35	0.00	0.00	0.07	0.00	0.00	0.45	2.47	0.45
Stilbella	2.97	1.03	1.11	0.85	0.40	0.00	0.00	0.08	0.00	0.00	0.47	2.44	0.47
Stilbella	3.00	1.00	0.89	1.03	0.44	0.00	0.00	0.08	0.03	0.00	0.57	2.44	0.64
Alternaria	3.45	0.55	1.45	0.14	0.00	0.78	0.00	0.00	0.07	0.08	0.15	2.37	0.36
Alternaria	3.85	0.15	1.40	0.15	0.00	0.71	0.00	0.00	0.05	0.00	0.16	2.25	0.25
Alternaria	2.86	1.14	0.79	0.29	1.17	0.00	0.00	0.00	0.18	0.00	0.34	2.25	0.69
Alternaria	3.10	0.90	1.73	0.00	0.51	0.00	0.00	0.00	0.00	0.00	0.17	2.24	0.17
Alternaria	2.99	1.01	1.50	0.00	0.73	0.00	0.00	0.00	0.00	0.00	0.31	2.24	0.31

Alternaria	3.82	0.18	1.43	0.11	0.00	0.65	0.02	0.00	0.05	0.07	0.14	2.22	0.30
Alternaria	3.81	0.19	1.40	0.13	0.00	0.68	0.00	0.00	0.06	0.08	0.15	2.22	0.35
Alternaria	3.25	0.75	1.27	0.17	0.77	0.00	0.00	0.00	0.08	0.00	0.14	2.21	0.29
Alternaria	3.87	0.13	1.41	0.12	0.00	0.67	0.00	0.00	0.05	0.09	0.12	2.20	0.32
Alternaria	3.86	0.14	1.44	0.12	0.00	0.63	0.00	0.00	0.05	0.10	0.11	2.19	0.32
Alternaria	3.80	0.20	1.56	0.08	0.00	0.55	0.00	0.00	0.04	0.07	0.12	2.18	0.28
Alternaria	3.82	0.18	1.53	0.10	0.00	0.55	0.00	0.00	0.05	0.06	0.13	2.18	0.29
Alternaria	3.81	0.19	1.55	0.10	0.00	0.53	0.00	0.00	0.04	0.08	0.11	2.18	0.28
Alternaria	3.86	0.14	1.57	0.08	0.00	0.50	0.00	0.00	0.05	0.00	0.16	2.16	0.25
Alternaria	3.82	0.18	1.51	0.10	0.00	0.55	0.00	0.00	0.05	0.06	0.20	2.15	0.37
Alternaria	3.25	0.75	1.73	0.00	0.42	0.00	0.00	0.00	0.00	0.00	0.32	2.15	0.32
Alternaria	3.21	0.79	1.39	0.17	0.58	0.00	0.00	0.00	0.12	0.10	0.21	2.14	0.55
Alternaria	3.13	0.87	1.39	0.00	0.75	0.00	0.00	0.00	0.00	0.00	0.46	2.14	0.46
Alternaria	3.12	0.88	1.40	0.33	0.40	0.00	0.00	0.00	0.26	0.00	0.31	2.13	0.82
Alternaria	3.00	1.00	1.45	0.00	0.66	0.00	0.00	0.00	0.19	0.00	0.29	2.11	0.67
Alternaria	3.87	0.13	1.59	0.11	0.24	0.00	0.06	0.00	0.05	0.08	0.11	2.00	0.29
Alternaria	3.83	0.17	1.53	0.11	0.27	0.00	0.07	0.03	0.06	0.07	0.12	2.00	0.31
Alternaria	3.85	0.15	1.52	0.13	0.28	0.00	0.07	0.00	0.06	0.11	0.13	2.00	0.36
Alternaria	3.86	0.14	1.65	0.08	0.24	0.00	0.02	0.00	0.04	0.07	0.11	2.00	0.26
Alternaria	3.83	0.17	1.67	0.08	0.25	0.00	0.00	0.00	0.05	0.08	0.10	1.99	0.27
Alternaria	3.81	0.19	1.62	0.10	0.23	0.00	0.04	0.00	0.04	0.16	0.13	1.98	0.38
Alternaria	3.87	0.13	1.62	0.06	0.24	0.00	0.06	0.00	0.06	0.09	0.10	1.98	0.31
Alternaria	3.89	0.11	1.59	0.08	0.26	0.00	0.05	0.00	0.06	0.08	0.13	1.98	0.32
Alternaria	3.89	0.11	1.57	0.08	0.24	0.00	0.07	0.02	0.05	0.10	0.12	1.97	0.32
Alternaria	3.93	0.07	1.56	0.12	0.25	0.00	0.03	0.00	0.06	0.07	0.12	1.97	0.32
Alternaria	3.81	0.19	1.64	0.09	0.24	0.00	0.00	0.00	0.05	0.13	0.14	1.97	0.37

Tetrahedral sheet: Si-Al^{IV}; Octahedral sheet: Al^{VI}-Ti; Interlayer cations: Ca-K.
Sum oct.: Total number of octahedral cations.
Int. charge: Total charge of the interlayer cations.
Orig. mica: average composition of pristine surface of the original mica.
Control: Individual analyses from control experiments.

Figure 1 new

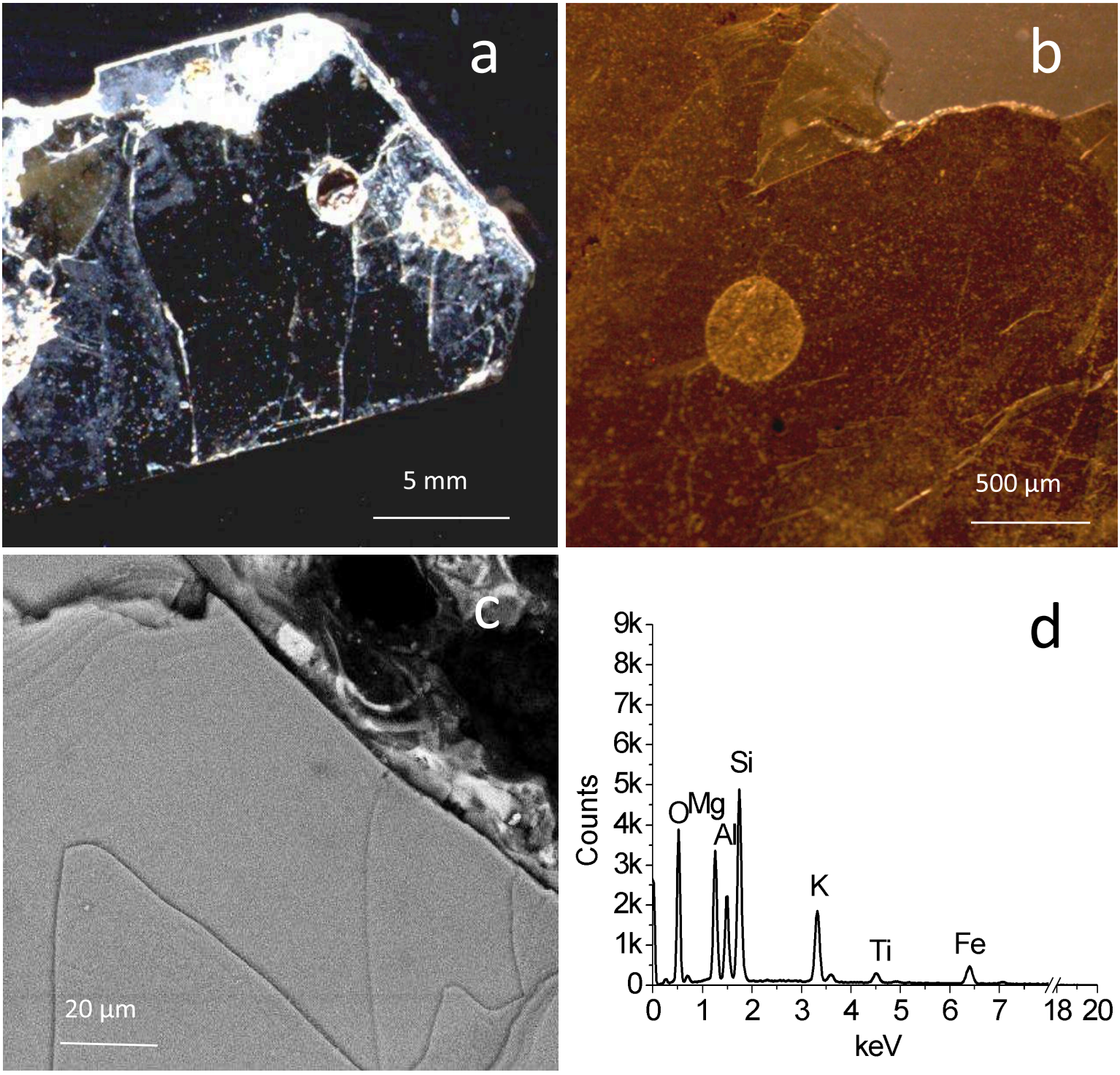
a
5 mm
b
500 µm
c
20 µm
d
Counts
9k
8k
7k
6k
5k
4k
3k
2k
1k
0
O
Mg
Al
Si
K
Ti
Fe
0 1 2 3 4 5 6 7 18 20
keV

Figure 2

Click here to download high resolution image

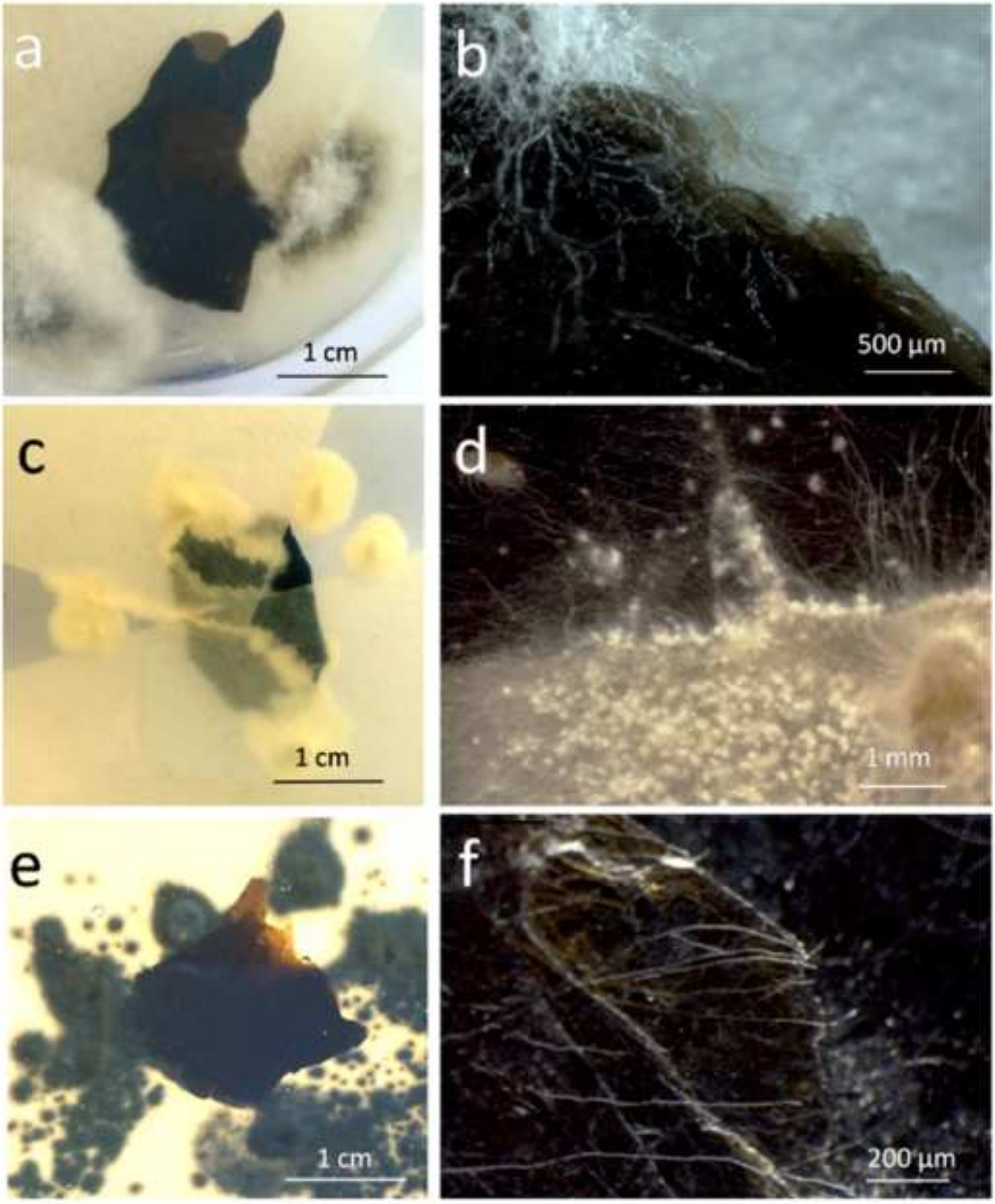

Figure 3

Click here to download high resolution image

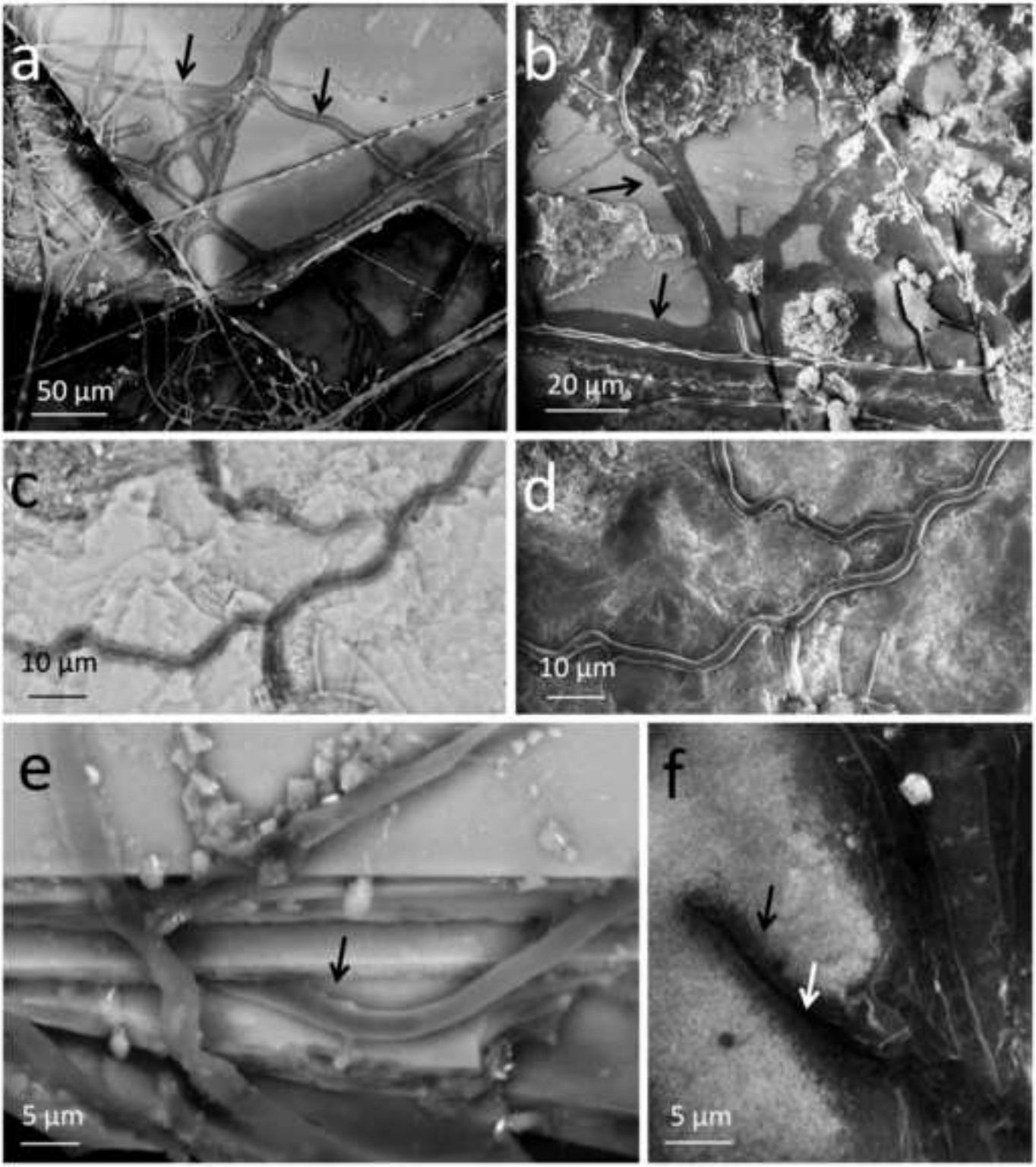

Figure 4

Click here to download high resolution image

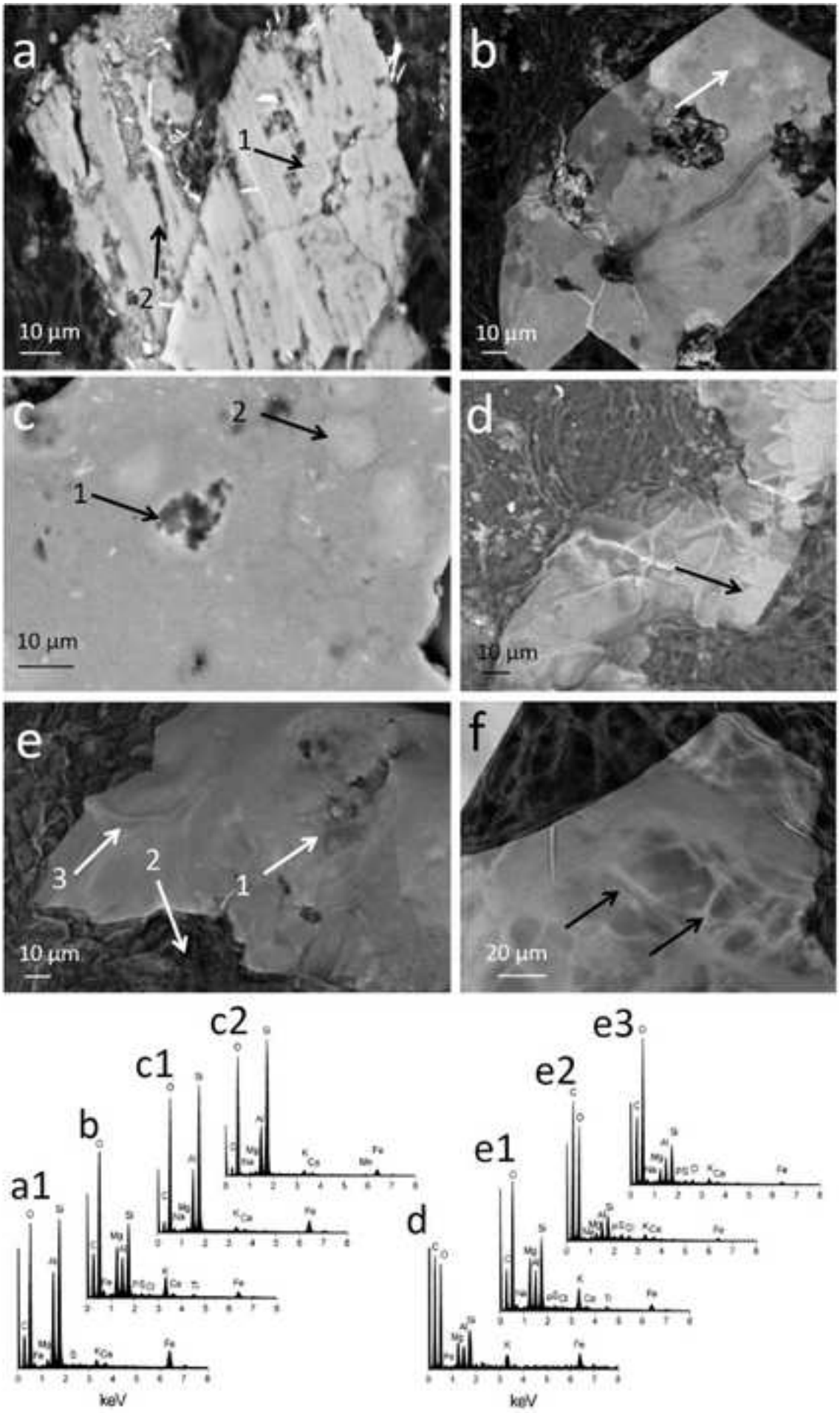

Figure 5

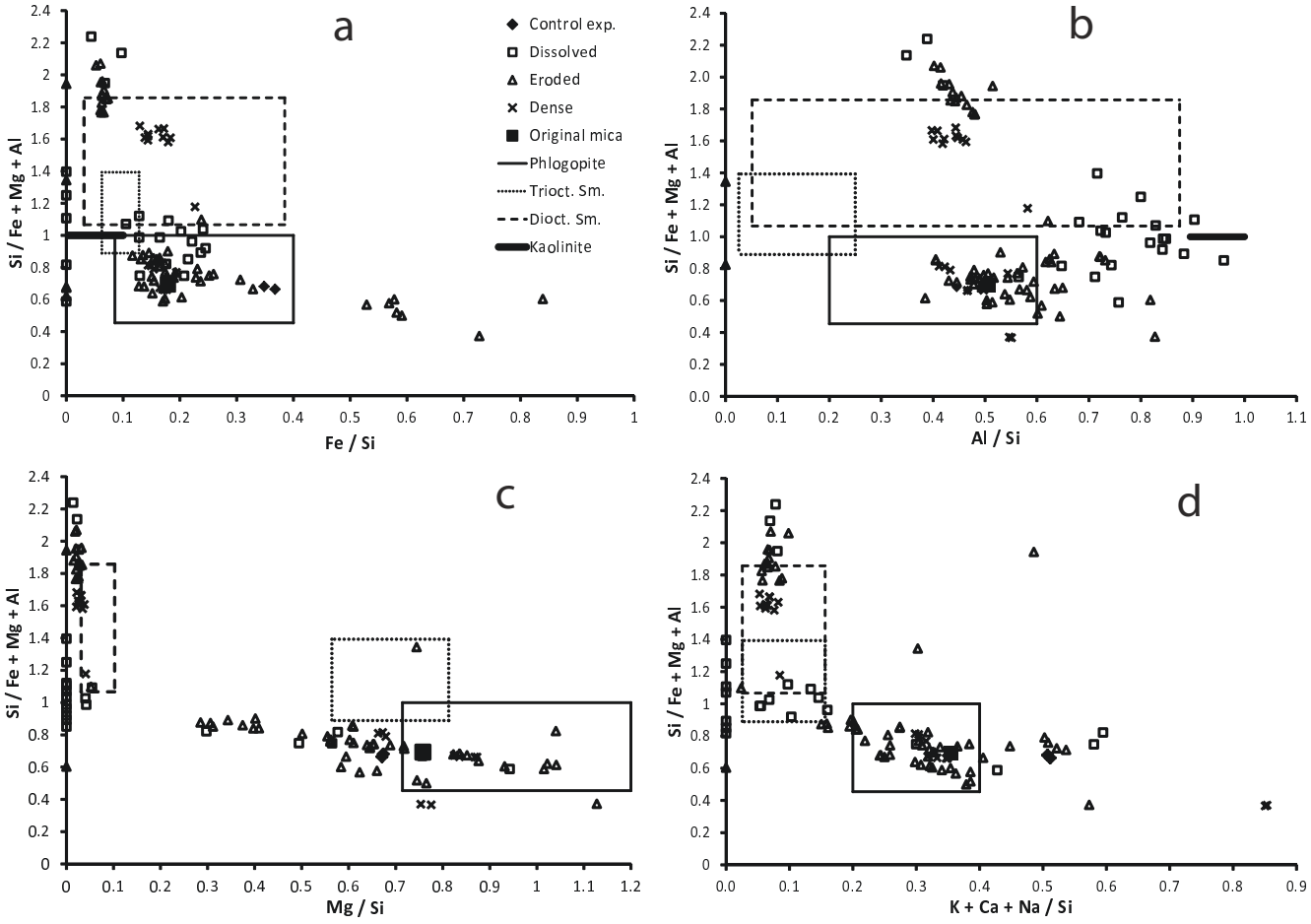

Fig. 5

Figure 6

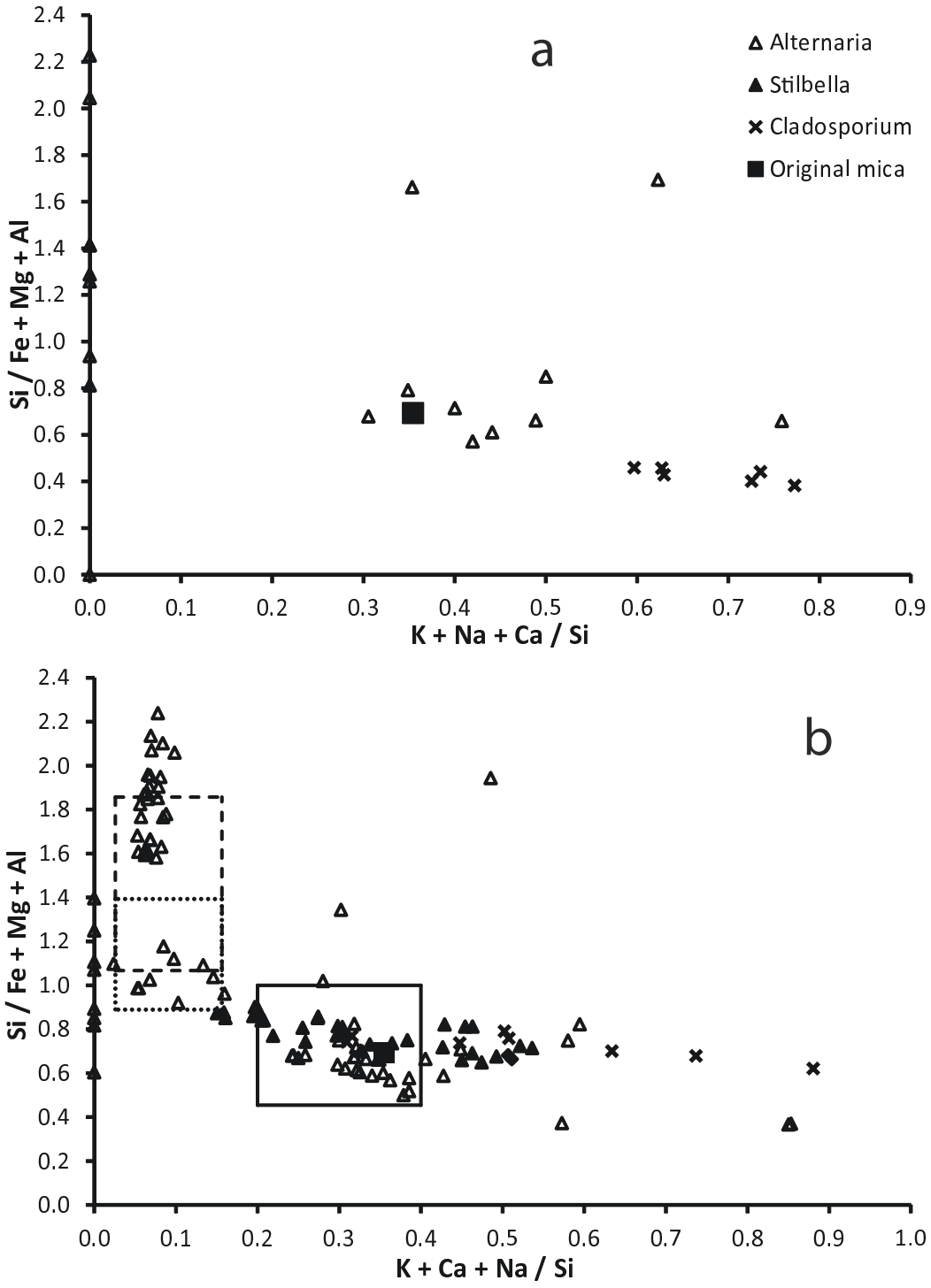

Fig. 6

Figure 7

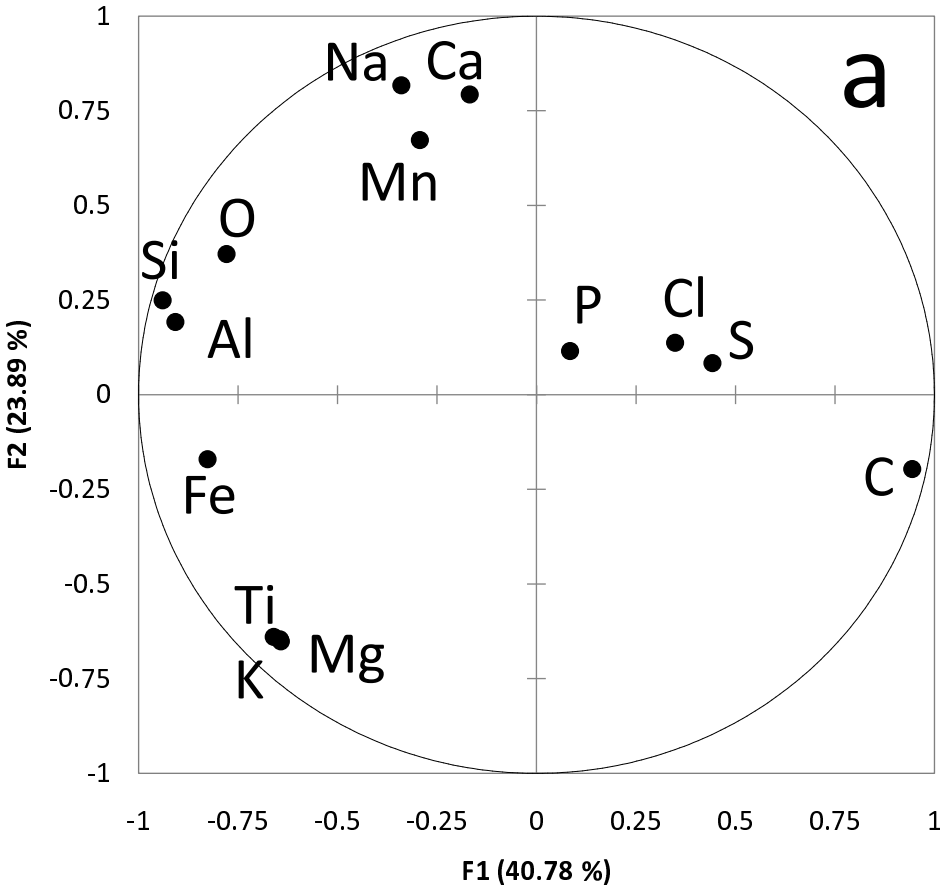
a
Na
Ca
Mn
O
Si
Al
P
Cl
S
Fe
C
Ti
Mg
K
F2 (23.89 %)
F1 (40.78 %)
1
0.75
0.5
0.25
0
-0.25
-0.5
-0.75
-1
-1
-0.75
-0.5
-0.25
0
0.25
0.5
0.75
1

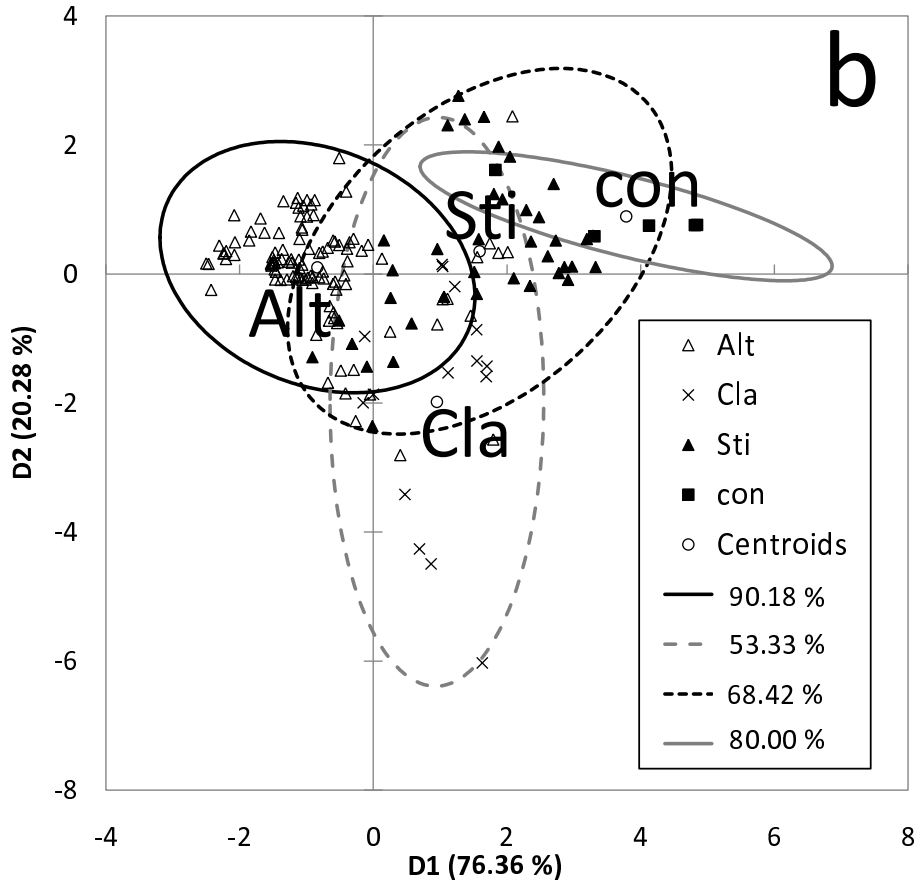
b
con
Sti
Alt
Cla
Alt
Cla
Sti
con
Centroids
90.18 %
53.33 %
68.42 %
80.00 %
D2 (20.28 %)
D1 (76.36 %)
4
2
0
-2
-4
-6
-8
-4
-2
0
2
4
6
8

Figure 8

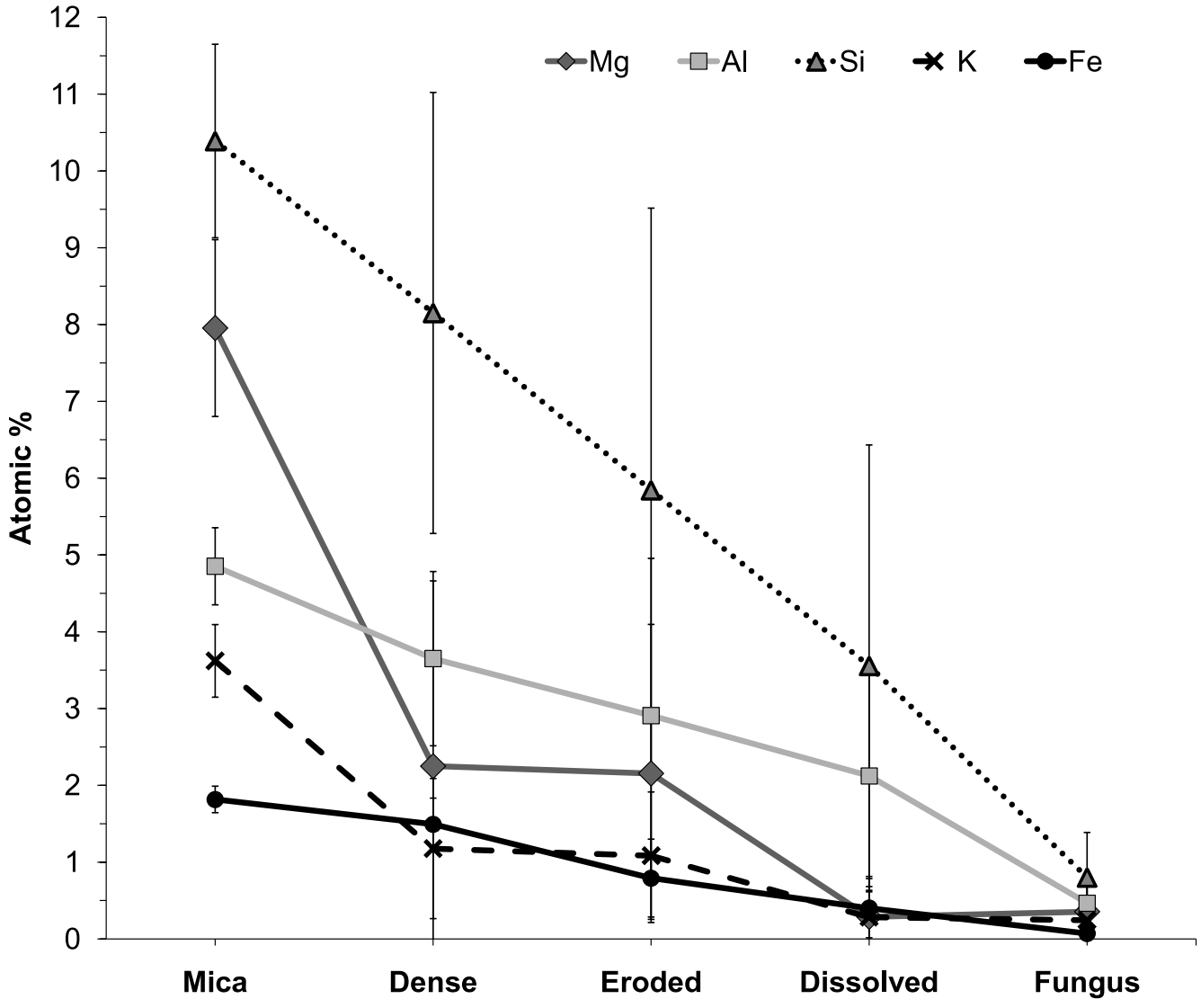
Mg
Al
Si
K
Fe
Atomic %
0
1
2
3
4
5
6
7
8
9
10
11
12
Mica
Dense
Eroded
Dissolved
Fungus

Supplementary Table S1

Click here to download Supplementary File: Supplementary data_Table S1.docx

Supplementary Table S2

Click here to download Supplementary File: Supplementary data_Table S2.docx

Supplementary Table S3

Click here to download Supplementary File: Supplementary data_Table S3.docx